UiT The Arctic University of Norway

Faculty of Science and Technology

Department of geosciences

Reconstruction of the paleoceanography west of Lofoten during the Last Glacial Maximum

Marthe Marie Mathisen

Master's thesis in *Marine Geology GEO-3900, May 2021*

Abstract

A 513 cm long sediment core from the Lofoten Contourite Drift at the continental slope west of the Lofoten Islands have been investigated. The aim was to reconstruct the paleoceanography during the Last Glacial Maximum (LGM). The Lofoten Contourite drift was relatively protected by the Lofoten Islands from the ice streams of the Scandinavian Ice Sheet during LGM.

An age model was constructed based on four ^{14}C dates from the core and correlations to nearby cores described in Vorren et al. (2015) and Weinelt et al. (2003). The core dates range throughout most of the LGM from at least 17,000 to 24,500 years BP.

The results are based on multiproxy analysis of the sediment core. Lithology log, x-ray, physical properties, grain size analysis, sortable silt analysis and IRD analysis was used to reveal the sedimentary processes, glaciation, and current speeds. The foraminifera analysis, Mg/Ca analysis and stable oxygen – and carbon isotope provides information about bioproductivity, ventilation, bottom environment, surface freshening and bottom water temperature. The core holds unique data. There are Mg/Ca samples for almost every ~100 years on average for the LGM record (~23-18.5cal. ka BP), so it is possible to resolve centennial changes, which is new for the LGM in the Nordic Seas.

The Mg/Ca showed a consistently cold Bottom Water Temperature (BWT) throughout the record. The bottom water temperature is colder than expected for the North Atlantic Intermediate Water during the LGM. The minima in the BWT correlate with low $\delta^{13}C$, low abundance of planktic and benthic foraminifera and reduction of the current strength. This may indicate intermediate water formation and interruption of the warm North Atlantic Intermediate Water. There is also a cold period between 20 and 19.8 cal. ka BP with high bioproductivity which is believed to a be a period with polynyas and mixed water masses.

Forord

Jeg vil først og fremst takke min veileder Tine Rasmussen for muligheten til å skrive oppgaven og for all hjelp og støtte. Ønsker også å takke Mohammed Ezat på institutt for geofag på Universitetet i Tromsø for å utføre Mg/Ca analysene og for hjelp til å forstå resultatene.

Takk til Trine Dahl, Ingvild Hald og Karina Monsen, for hjelpen på laboratoriet. Ønsker også å takke institutt for geofag for økonomisk støtte for å gjennomføre laboratoriearbeidet.

Takk til mannskapet på R/V Helmer Hansen og de som var med ombord som hentet opp kjernen.

En spesiell takk går til alle foreleserne på Universitet i Tromsø og Universitet i Oslo som har delt sin geofaglige visdom, entusiasme og geoglede. I forelesningssal, i felt og på tokt. Til foreleseren som dro med seg den samme tunge steinen på forelesning fram til noen gjettet hva det var. At det var en rød sandstein fra Brumunddal glemmer jeg nok aldri. Jeg har fått blitt kjent med Oslofeltet, Finse, Troms og Svalbard gjennom forelesere som peker, tegner og forklarer både i sol, motvind og regn (stort sett det sistnevnte). Tusen takk til foreleserne som lagde vel gjennomtenkte emner og som ga personlige tilbakemeldinger. Dere har gjort studietiden lærerik og morsom.

Takk til familie og venner. Mannen min som har vært ved min side og dattera som fått oss opp tidlig tidlig på morgenen, alltid med et smil. Matilde du er sola og hjertet mitt.

Marthe Marie Mathisen

Table of Contents

1 Introduction

The aim of the study is to investigate the oceanographic and glacial conditions west of Lofoten during the Last Glacial Maximum.

2 Background

2.1 Study Area

The study area is located at the continental slope west of the Lofoten Islands, northern Norway (Figure 1). Compared to other margins of Norway, the margin of Lofoten is characterized by a relatively narrow shelf (~10-80 km) and a steep continental slope (up to 10°) (Laberg et al., 1999, Vorren et al., 2015). At the site the continental slope is 3-5°(Rise et al., 2013). The continental slope is in general dominated by trough mouth fans and canyons (Kenyon, 1987, Rydningen et al., 2013). The troughs worked as drainage routes for the ice streams from the Scandinavian Ice Sheets, the largest shelf crossing trough, the Vestfjorden-Trænadjupet (Figure 1) was one of the main drainage routes of the Scandinavian Ice Sheet (Ottesen et al., 2005, Vorren et al., 2015). The Lofoten Islands have acted as a sediment barrier and have been routing most of the fluvial and glacial sediments south and north of the study area (Ottesen et al., 2005). The main sediment input has been transported along the slope, defined as a contourite drift and termed the 'Lofoten drift' (Laberg et al., 1999, Vorren et al., 2015).

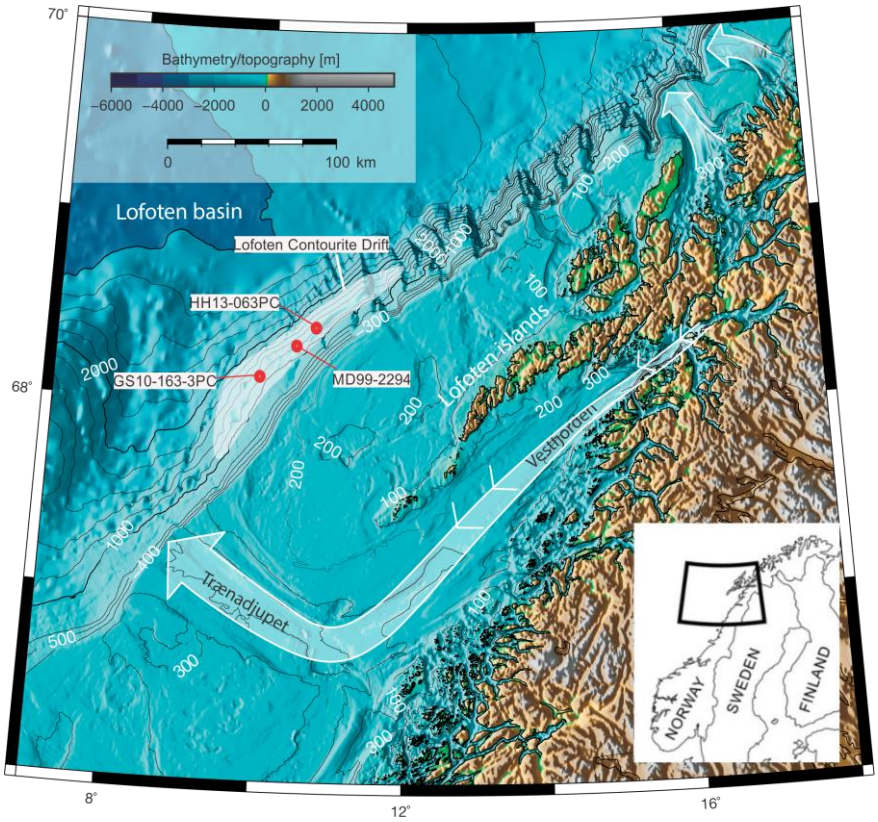

Figure 1 Map of Lofoten in Northern Norway. Lofoten Contourite drift is marked in white. The examined core HH13-063PC is the northernmost red dot. MD99-2294 and GS10-163-3PC are two neighbour cores respectively 18.5 and 240 km southeast of HH13-063PC.The neighbouring cores are described in other papers (e.g. Rørvik et al. (2010) and Baeten et al. (2014)). Modified from Vorren et al. (2015).

Above the site there is a canyon recognized in Rise et al. (2013). This is the first canyon of a series of 15 canyons on the steep slope of Lofoten-Vesterålen (Figure 2). The canyon above the site is named canyon 1 in Rise et al. (2013). Canyon 1 starts below the shelf break and is 10 km long, it has a width of 2-2.5 km on the top and 0.6-0.9 km wide at the bottom. The maximum slope angle at the canyon head is 15 °. The canyon above the site does not reach the shelf break, so it is thought to have been created by upslope retrogressive erosion. The Lofoten contourite drift is affected by sliding below 1400-1500 meters depth. There are several slide escarpments, marked with white dashed lines in Figure 3 close to core HH13-063PC. The placement of core HH13-063PC in Figure 3 is not exact since it was manually placed based on distance and angle from MD99-2294 which was put in the figure of Rise et al. (2013).

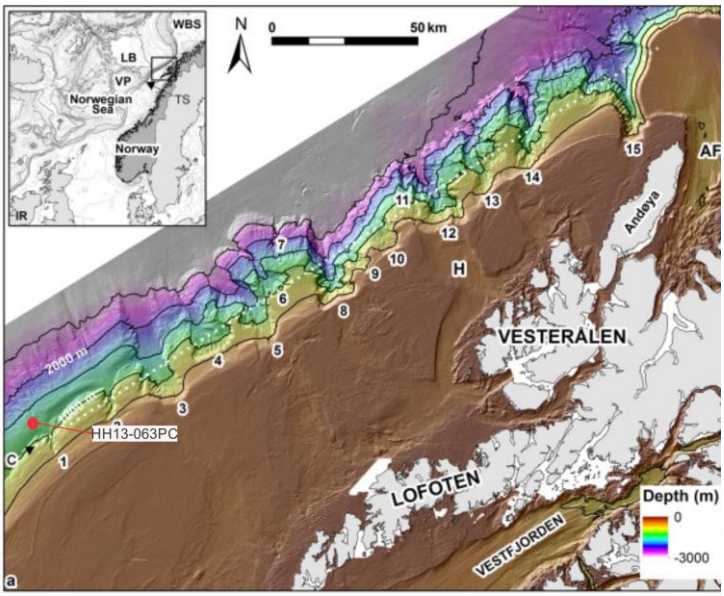

Figure 2 High-resolution bathymetric relief image of the Lofoten-Vesterålen margin. HH13-063PC is marked with a red dot and is situated below canyon number 1 of 15 canyons along the margin. Modified from Rise et al. (2013)..

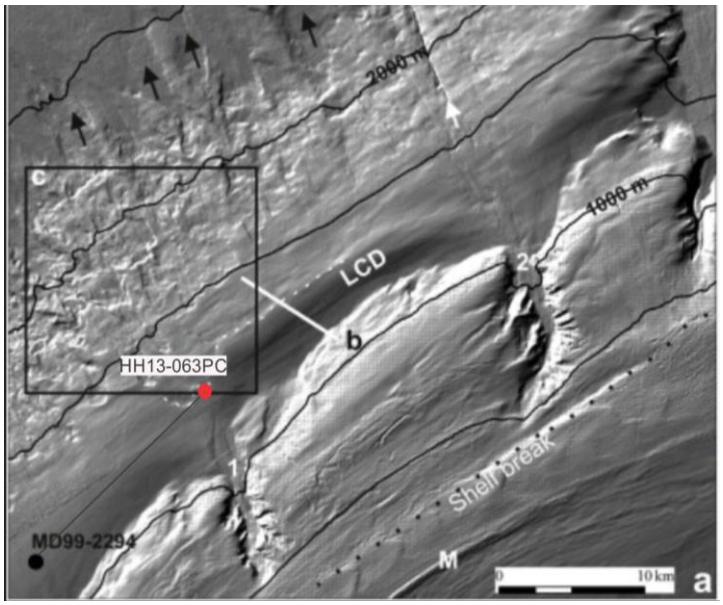

Figure 3 Shaded relief image. The white dashed line is a buried slide escarpment. The red dot is the location of HH13-063PC, while the black dot is MD99-2294. M is a moraine ridge on the outermost shelf. (LCD= Lofoten Contourite Drift)

2.2 Lofoten drift

The Lofoten drift was first described by high-resolution and multichannel seismic data in Laberg et al. (1999). The contourite drift was later in Laberg et al. (2001) classified as a mounded, elongated, upslope accretion drift. The drift is separated, has an elongated shape with a mound and is migrating upward the slope (Figure 4).The Lofoten drift is situated downslope of the steepest part of the continental slope deeper than 1000 meters water depth. It continues along-slope for at least 90 km (Figure 1). The contourite drift consist mainly of along-slope sediments originating from winnowing of the shelf and the upper slope. By using high-resolution and multichannel seismic data the maximum thickness of the contourite drift was found to be 360 meters (Laberg et al., 1999). The upper part (~24 meters) of the drift consists mainly of clay (50-60%) and silt (40-50%), and is alternating between homogeneous and laminated sequences (Laberg and Vorren, 2004, Rørvik et al., 2010). Minor fractions of sand are found throughout the upper part and are interpreted to be ice-rafted debris. Most of the IRD are believed to have originated from the Vestfjorden-Trænadjupet paleo ice stream, but a small fraction of the IRD stems from northward floating icebergs from the Norwegian Channel Ice stream (south of Norway) (Rørvik et al., 2010). The drift has apparently been little affected by downslope processes (Laberg et al., 1999)

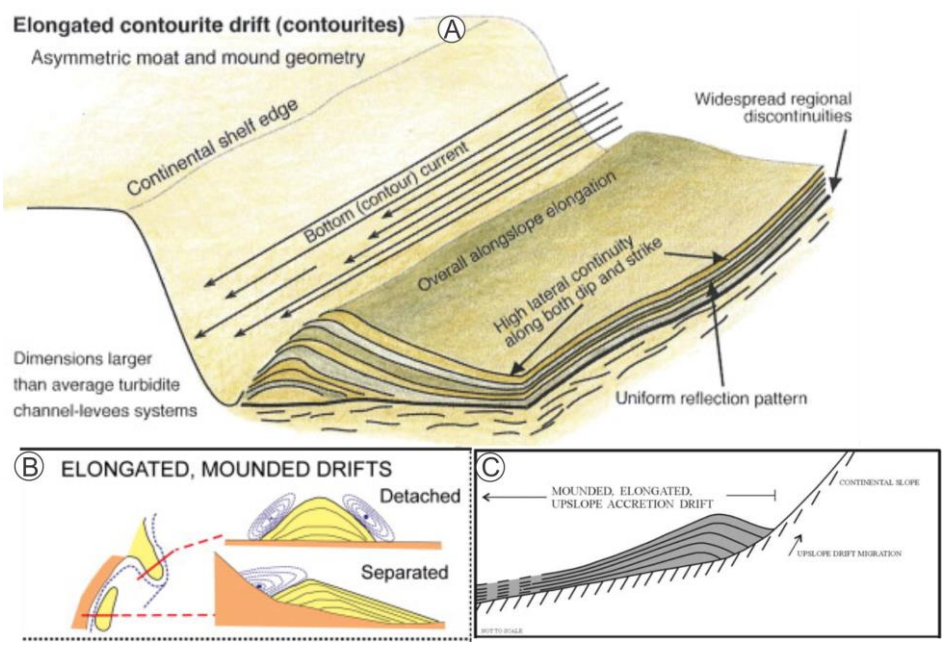

Figure 4 a) The bottom current is following the contour of the slope. b) the Lofoten drift is a separated drift. C) the drift has an upslope drift migration. Making the Lofoten drift a mounded, elongated, (separated), upslope accretion drift.

2.3 Modern ocean circulation

The North Atlantic Ocean's thermohaline circulation is a principal modulator of the global climate system. The inflow of warm saline water from the North Atlantic into the Arctic gives excess heat and moderates the regional climate. Most of the heat is released in the Nordic seas, the cooling leads to a dense water formation and overturning circulation, constituting the northernmost limb of the Atlantic Meridional Ocean Circulation (AMOC) (Figure 5). The newly generated cold deep water overflows the Greenland-Scotland Ridge which separates the Nordic seas from the Arctic Ocean. The cold, dense water mixes with warmer water in the Atlantic and becomes North Atlantic Deep Water (NADW). The overflow occurs via the Denmark Strait, Iceland-Faroe Ridge and the Faroe-Shetland Channel (Hansen and Østerhus, 2000)

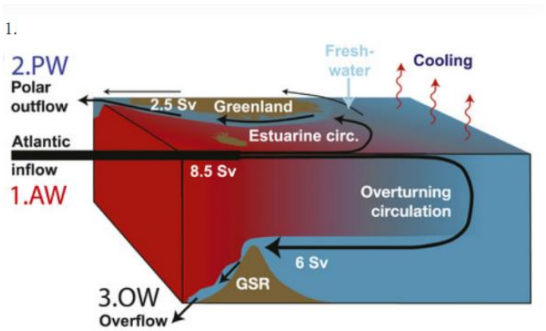

Figure 5 The thermohaline circulation. (GSR= Greenland-Scotland Ridge) From Hansen et al. (2008) and Eldevik and Nilsen (2013)

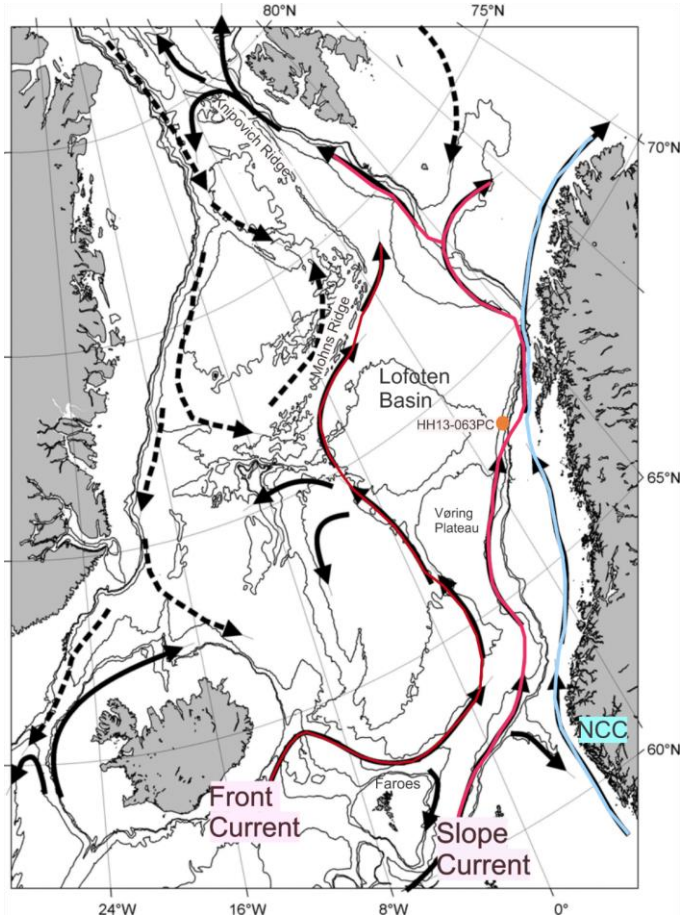

Figure 6 The Upper layer circulation in the Nordic seas. HH13-063 is marked with an orange dot. The solid lines are Atlantic water, while dashed lines are Arctic and Polar waters. The red lines are representing the two branches of Atlantic Current: Front Current and Slope Current. Blue line is Norwegian Coast Current. Modified from Orvik and Niiler (2002) and Blindheim (2005)

Orvik and Niiler (2002) recognise two main pathways of Atlantic Water into the Nordic seas and towards the Arctic Ocean. The newer described western branch (the Front Current) is extending from the Iceland-Faroe Ridge to the Fram Strait. The Front Current is following the topography and the slopes of the Vøring Plateau, follows the Mohns Ridge and Knipovich Ridge into the Fram Strait (Orvik and Niiler, 2002).

The eastern branch (the Slope Current) goes through Rockall Trough and the Faroe-Shetland Channel on the eastern side of the Faroe Islands before it continues along the Norwegian coast. The Slope Current splits into two branches north of the Lofoten basin, one branch turns into the Western Spitsbergen Current and the other into the North Cape Current. The Slope Current dominates the upper ca 800 meters of the water column (Blindheim, 1990)

The Slope Current accelerates along the steep continental slope of Lofoten (Poulain et al., 1996), where it gets squeezed together with the Norwegian Coast Current. The Norwegian Coast Current consists of relatively buoyant coastal water which stems from the Baltic Sea and from Norwegian river run off. The different hydrographic properties of the two water types do set up conditions for flow instabilities (Ghaffari et al., 2018).

In recent years several studies have been conducted about the unstable current off the Lofoten Islands. Ghaffari et al. (2018) studied the influence of the steep topography and found that the Slope Current is both barotropically and baroclinically unstable. The Lofoten basin northwest of the core site are described in Eldevik and Nilsen (2013) as the most intense mesoscale eddy field in the Nordic Seas, and an important component in the AMOC. The slope current along the Lofoten Escarpment next to the site is being examined in Fer et al. (2020).

Arctic Intermediate Water (AIW) is found between 800-2000 meters water depth west of the Lofoten Islands. AIW is characterised by a slight salinity minimum and origin from the northern Icelandic slope in the Iceland Sea by convection here to intermediate water depth. It has a temperature range between -0.5 - 1.0°C. The intermediate water keeps the Atlantic surface water from mixing with the deep water (Blindheim, 1990). The velocity of the

surface water is measured to be 1.1 m/s at 15 meters depth, while the intermediate water is slower with an average velocity between 0.2-0.4 m/s, with the lowest velocity at 1044 meters water depth (Poulain et al., 1996, Heathershaw et al., 1998)

The bottom water, below 2000 meters in Lofoten basin, enters from northwest across the mid-ocean ridge north of Jan Mayen and is a mix of deep water from the Arctic Ocean and deep water formed in the Greenland Sea (Swift and Koltermann, 1988).

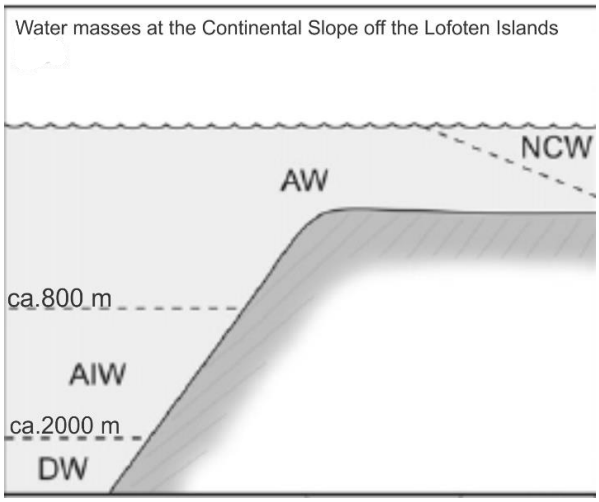

Figure 7 Distribution of the water masses at the continental slope West of the Lofoten Island. (NCW=Norwegian coastal water, AW=Atlantic Water, AIW=Arctic Intermediate Water, DW=Deep Water) Modified from Rørvik et al. (2010), (Orvik and Niiler, 2002).

Figure 8 shows the temperature profile at the margin of Lofoten-Vesterålen during spring/summer. At more than 1000 meters depth the temperature is circa 0°C.

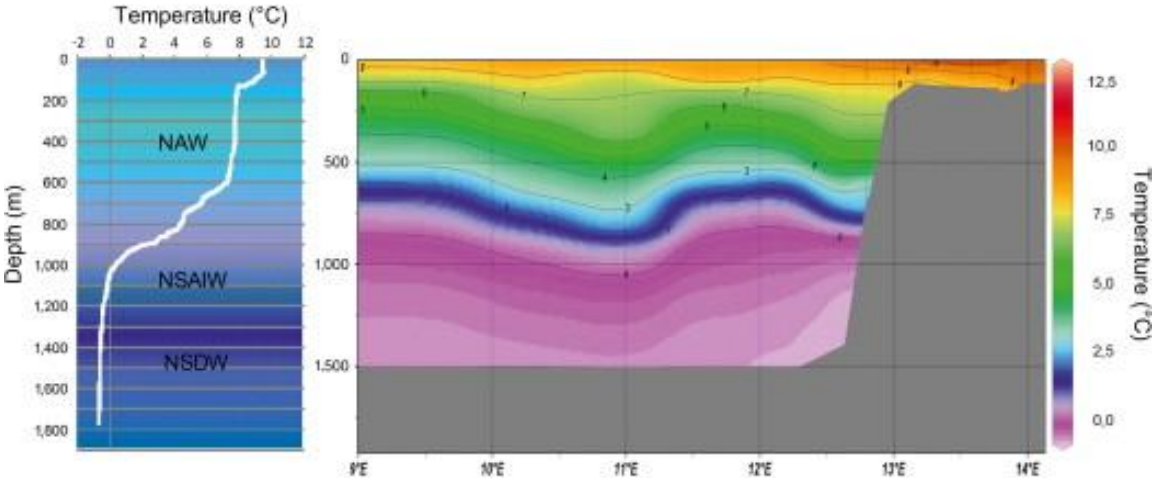

Figure 8 Temperature profile and bathymetrical distribution of the water masses. Temperatures are decreasing rapidly from 600 to 1000 meters. Below a thousand meters it is stabilising at circa 0 °C. This varies over seasons. The graphs show spring/summer temperatures. From Buhl-Mortensen et al. (2012)

2.4 Last Glacial Maximum (LGM)

The Last Glacial Maximum (LGM) is conventionally defined by the sea level record since it caused a large global sea level fall. The global sea level fall gives a maximum $\delta^{18}O$ value. So, the peak of $\delta^{18}O$ values is defined as the LGM. The sea level records from far-field sites (e.g. New Guinea and Barbados) sets the timing of the LGMs from 26.5 to 19.0 ka. There are considerable regional variations (Clark et al., 2009).

In the Lofoten-Vesterålen area the Local Last Glacial Maximum (LLGM) started when the Scandinavian Ice Sheet reached its maximum and extended to the shelf break, in the vicinity of the Trænadjupet, south of the study area around 26.0±0.5 cal. ka BP (Dahlgren and Vorren, 2003). The ice sheet started to retreat from the shelf break between 19 and 17.5 cal. ka BP (Dahlgren and Vorren, 2003, Hjelstuen et al., 2004). The last interglacial event within the LGM with colder temperatures and advances of ice sheet lasted to 16.3 cal. ka BP (Vorren et al., 2015)

Heinrich events are when large icebergs were discharged from the North American ice Sheet into the Atlantic Ocean between 40° and 55 °N (Heinrich, 1988). It is proposed that the Heinrich event 1 was triggered by reduced North Atlantic Deep Water formation which warmed the North Atlantic subsurface water (Álvarez-Solas et al., 2011).

2.4.1 Climate

The first study of paleoenvironmental development during LGM in Andøya, northern Norway was published in 1979 by Vorren and Elvsborg (1979). More than 30 years later several papers have investigated the climate and glaciation history in the area. Vorren et al. (2013) reviewed the studies and re-evaluated the chronology and climate from 22.2 to 14.4 cal. ka BP.

There was a dry, high arctic climate. The mean July air temperature was fluctuating between 0°C and 3°C between 22.2 and 14.5 cal. ka BP. There were three warm periods: 21.4-20.1, 18.8-18.1, around 17 and from ca.16.4 cal. ka BP onwards. The climate regime shifted rapidly between these warmer and colder periods between 22.2 and 14.5 cal. ka BP, in probably less than a couple of decades (Vorren et al., 2013)

2.4.2 Glacial History

Glacial landforms onshore and offshore have been analysed to recognise glacial events in the Andøya area and on the continental shelf off Lofoten-Vesterålen. Large grounding zone wedges and end moraines have been used to reconstruct glacial events of stillstand, advances and retreats onshore and offshore Andøya.

Five main glacial events have been recognised (Vorren et al., 2015), where four of them are within the timespan of this thesis (c. 24 – 17 cal. ka BP).

- The Egga events (Egga I and Egga II) are the outermost moraines located at the shelf edge and are interpreted to represent the maximum extent of the ice sheet. It is believed that it did not reach to the shelf edge above the Lofoten drift (Figure 9). Egga II overrides Egga I, it is thought that Egga I is from before 24 cal. ka BP while Egga II is from ca. 23-22.2 cal. ka BP (Vorren et al., 1988, Vorren and Plassen, 2002, Rydningen et al., 2013, Vorren et al., 2013).
- The Endleten event dates from 22.2 to 18.6 cal. ka BP (Vorren et al., 1988, Vorren et al., 2013). The moraine is parallel to the moraine from the Egga events. It is unknown if it reached to the shelf break. It separates and bends east and landwards above the Lofoten drift (Figure 9).
- The Flesen event is dated to be from 18 to 17.5 cal. ka BP (Vorren and Plassen, 2002, Vorren et al., 2015) and the moraine is located on the shore-side of the previous events.

Between the main glacial events were warm interstadials events; the Andøya interstadial (23.5 cal. ka BP) and the Endleten-Flesen (E-F) inter-event period (c. 18 cal. ka BP) (Vorren et al., 2015).

The sediments were transported to the shelf break as till wedges and brought via fast-flowing ice streams and redistributed down the paleo slopes as gravity flows (Ottesen et al., 2005) One of the main drainage routes for the Scandinavian Ice sheet in North Norway is the outlet at Trænadjupet. Here, the Ice sheet reached the shelf break at c. 24.6, 22.3, 21.1, 20.2, 18.7 cal. ka BP ((Dahlgren and Vorren, 2003).

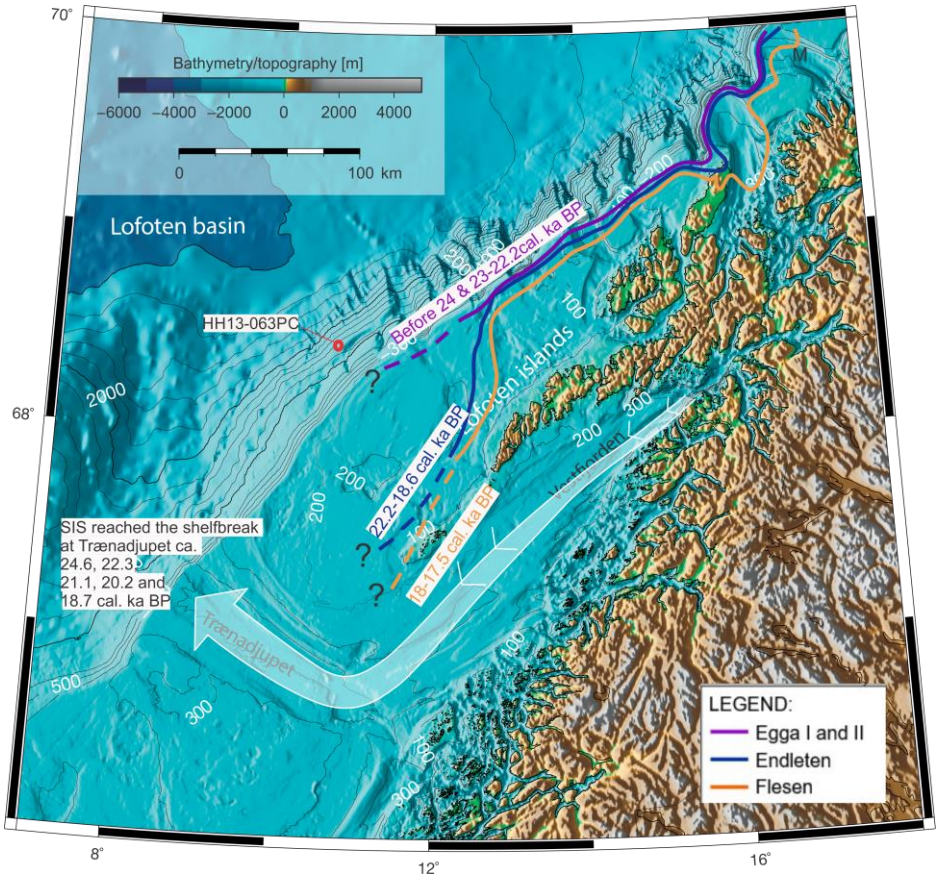

Figure 9 Glacial extension by end moraines. The events are from Vorren et al. (2015), the dates for Scandinavian Ice Sheet reached the shelf break is from Dahlgren and Vorren (2003). Modified from Vorren et al. (2015)

The Scandinavian Ice Sheet at the continental shelf above the Lofoten drift was probably thinner than south and north of the site, due to the damming effect (Laberg et al., 1999, Laberg and Vorren, 2004). Vorren et al. (2015) concludes with no evidence of the ice sheet ever reaching the shelf break above the Lofoten Drift.

2.4.3 Oceanography

The MARGO (Multiproxy Approach for the Reconstructions of the Glacial Ocean) project with more than 50 scientists was aimed at reconstructing the global Sea Surface Temperature (SST) and sea ice during LGM. They generally concluded that the largest cooling occurred in the central Atlantic, and that the cooling was larger in the eastern part than in the western part of the North Atlantic. The Nordic seas was ice-free during summer, allowing a direct heat and moisture transfer between surface water and the continents building up continental ice sheets (Hebbeln et al., 1994, Sarnthein et al., 2003, MARGO Project Members, 2009).

The formation and disintegration of the ice sheets that surrounded the North Atlantic together with the presumably widespread winter sea-ice cover during the LGM had a significant influence on oceanic conditions, atmospheric circulation, hydrological balance and sedimentation (Mix et al., 2001, Rørvik et al., 2010). There is probably a causal link between the Atlantic Meridional Ocean Circulation (AMOC) and climate swings during the last glacial cycle (Rahmstorf, 2002).

The Atlantic surface water inflow during the LGM was unstable and had a large variability in salinity and temperature (Weinelt et al., 1996). This may indicate it was interrupted by meltwater supplies (Lekens et al., 2006). Two or three times the intruding freshwater input was so massive it is believed it impacted the intermediate water formation in the Nordic Seas and a reduced the AMOC (Rørvik et al., 2010, Rørvik et al., 2013).

The AMOC seems to have weakened during the cold stadial, but not stopped, because there is evidence of inflow of Atlantic water throughout the glacial periods where the Atlantic surface water shifts from surface to subsurface or intermediate water (Ezat et al., 2014). In response to the AMOC weakening several studies have shown a warming of subsurface and intermediate water (Rasmussen and Thomsen, 2004, Marcott et al., 2011, Ezat et al., 2014). It is believed that at some point in time the warm subsurface water started to rise, creating a vertical shift in the water masses which is reflected in warmer SST and colder BWT (Marcott et al., 2011, Ezat et al., 2014) The warming of the subsurface water was possibly a trigger for ice sheet instability and could produce a Heinrich event (Marcott et al., 2011).

The strength and placement of the deep ocean convection during the LGM has been debated and modelled several times. Previously, it was thought that the main convection occurred south of Iceland and was only producing Intermediate water called Glacial North Atlantic Intermediate Water (GNAIW) (Duplessy et al., 1988, Duplessy et al., 1991, Boyle and Keigwin, 1987, Oppo and Lehman, 1993). Later, studies placed the convection and production of North Atlantic Deep Water in the north polar subpolar gyre (Keigwin and Swift, 2017), in the Norwegian Sea (Schäfer-Neth and Paul, 2001) or the North Atlantic as today (Howe et al., 2016). However, the deep convection is believed to be weak and unstable with an intermittent overflow across the Greenland-Scotland Ridge. (Lynch-Stieglitz et al., 1999, Rasmussen et al., 2002, Crocket et al., 2011) A recent data-based study by Seidenkrantz

et al. (2021) supports the hypothesis of Howe et al. (2016) of a strong Meridional Overturning Circulation cell in the North Atlantic during LGM.

The LGM is characterized by stable and stratified hydrographic conditions (Rasmussen and Thomsen, 2004, Ezat et al., 2014). with warm subsurface temperatures, more than 2 °C due to inflow of Atlantic Water (Rørvik et al., 2013). The deep Nordic seas was on average 1.5 °C warmer during LGM than modern temperatures (Ezat et al., in revision, Paleoceanography and Paleoclimatology).

2.5 Sedimentation processes

2.5.1 Along-slope processes

Along-slope currents are related to erosion, sediment transport and deposition on continental margins. Contourites was first described circa 50 years ago. There is still a lack of detailed knowledge about the sedimentological and oceanographic processes shaping the deposits. There is also a need of agreement on common classifications of contourites (Rebesco et al., 2014). Contourites were first defined as sediments deposited by thermohaline-induced geostrophic currents, i.e. contour currents. Later a broader definition was added; “sediments deposited or substantially reworked by bottom currents”. (Stow et al., 2002, Rebesco and Camerlenghi, 2008). Rebesco and Camerlenghi (2008) define a contourite drift as the sedimentary deposit of the contour currents. Contourite drifts usually have a fairly continuous sediment record with a high time resolution. Therefore, they give valuable information about ocean circulation, current velocities, ice-sheet stability and more (Rebesco et al., 2014).

2.5.2 Ice-Rafted Debris

Ice-rafted detritus (IRD) occurs in areas with sea ice or icebergs. The IRD consists of coarse grained material released from melting ice and is found on the sea floor (Ruddiman, 1977). Iceberg rafted IRD is generally coarser than sea-ice rafted and can be transported for a longer distance (Dowdeswell and Dowdeswell, 1989, Gilbert, 1990). IRD is used as a proxy for glacial activity and glacial outreach. Massive input of IRD recorded as thick layers of iceberg rafted debris can indicate Heinrich events (Heinrich, 1988, Bond et al., 1993)

These layers stretch across the entire North Atlantic Ocean north of 45N. Counterpart layers have been found in the Nordic seas that correlate in time with the deposition of Heinrich layers in the North Atlantic Ocean (e.g., (Fronval et al., 1995, Rasmussen et al., 1996, Weinelt et al., 2003)

2.5.3 Meltwater plumes

When meltwater originating from below or inside a glacier (subglacial or englacial) enters the water column it tends to float upwards due to upwelling caused by lower density. The upwelled sediment loaded meltwater will with momentum forces move horizontal as a jet. As the meltwater jet mixes with the surrounding water it will lose density and become more buoyant and transform from a meltwater jet to a meltwater plume. The coarsest material as sand and coarse silt will first deposit while finer particles will stay longer in suspension, creating a distal fining from the glacier. The meltwater is discharged in pulses, so the sediments can settle as parallel laminated layers (Ó Cofaigh and Dowdeswell, 2001)

2.5.4 Downslope processes

Downslope processes are gravity driven processes which re-deposits sediments on the continental slope or in the deep-sea basin. The processes include creeping, sliding, slumping, turbidity currents and debris flows. The Scandinavian Ice Sheet pushed glaciogenic diamictons in front of it towards the shelf break. These sediments were later re-sedimented down slope by gravity flows (Dahlgren et al., 2002).

2.6 Foraminifera

Foraminifera are a large order of unicellular protozoans classified to the supergroup Rhizaria. Rhizaria are characterized by a psedupodia, an armlike or weblike outgrowth, which can be used to trap food, for movement or for anchorage (Cavalier-Smith and Chao, 2003). Foraminifera lives either in the upper water masses as the planktic type or at the seabed as the benthic type. The protoplam is enclosed by a protective test. For most species the test is built from calcium carbonate ($CaCO_3$) taken from the ambient seawater, but some benthic species have tests made of agglutinated materials, i.e. sand grains, sponge spicules, other foraminifera and tephra particles amongst others. Traditionally, the morphology of the test has been an important tool for classification of the group, but newer classification systems are evolving based on genetics (Pawlowski et al., 2013). Foraminifera are preserved as microfossils in the marine sediments and living foraminifera today make up 55% of the Arctic biomass and 90% of the deep sea biomass (Armstrong and Brasier, 2013). Foraminiferal shells, the carbonate ooze, plays an essential role in the carbon cycle and is a valuable proxy for reconstruction of past oceanography and environment (Kimoto, 2015). The foraminifera is the most commonly used proxy in paleoceanography, either from the fossil assemblage or through the extraction of chemical signals from the shell (Kucera, 2007, Sejrup et al., 2004). “These inconspicuous organisms and their tiny shells are the true heroes of our quest to reveal the past of our planet”(Kucera, 2007).

2.6.1 Planktic foraminifera

Planktic foraminifera live at the surface and down to a 1000 meters depth. Quaternary planktic species consist of less than 30 species and are primary controlled by temperature, salinity and nutrients (Kimoto, 2015, Sejrup et al., 2004). During the LGM there was a high productivity and a high concentration of planktonic foraminifera (Hebbeln et al., 1994, Dokken and Hald, 1996).

Neogloboquadrina pachyderma

Neogloboquadrina pachyderma is the specie that dominates in the polar high latitudes. *N.pachyderma* is found to correlate with water masses and latitude. They generally prefer low water temperature, low salinity and high food availability (Ericson, 1959, Kohfeld et al.,

1996, Bé and Hutson, 1977). *N.pachyderma* has a left coiling, while the variant with a right coiling was found to be another specie, *N.incompta,* which are found at lower latitude with warmer water (Darling et al., 2006). *N.pachyderma* can adapt its living depth in the water column, but are mainly found between 50-200 meters in ice free waters (Simstich et al., 2003, El Bani Altuna et al., 2018).

2.6.2 Benthic foraminifera

The benthic foraminifera live on or within the seafloor at all depths. There are about 5000 known living species. The assemblage of benthic foraminifera may indicate water depth, temperature, proximity to glaciers, bottom water circulation and current strength, substrate and several other environmental parameters (Sejrup et al., 2004, Armstrong and Brasier, 2013).

2.6.2.1 Arctic benthic foraminifer species

The main habitat of *Cassidulina neoteretis* is the arctic and cold boreal region. It is most common between 1000 and 1500 meter water depth (Seidenkrantz, 1995). *C.neoteretis* is often associated to cooled North Atlantic intermediate water with temperatures -1 to 2 °C in slopes (Jennings and Helgadottir, 1994) They are present in seasonally ice-free areas but rare in permanently ice-covered sites. *Cassidulina neoteretis* responds to phytoplankton blooms. (Jennings and Helgadottir, 1994, Kristjánsdóttir et al., 2007).

2.6.2.2 Atlantic benthic foraminifer species

This is a group put together of relatively rare species in the North Atlantic that are normally found south of the Faroe Islands with temperatures higher than 2 °C. When found in the north Atlantic they can be used to pinpoint interstadials (Rasmussen et al., 1996, Rasmussen et al., 2003) '*Sigmoilopsis schlumbergeri, Eggerella bradyi, Bulimina costata, Cibicidoides aff. Floridanus* are all included in this group

3 Material and methods

The study is based on marine sediments from a piston core. The core HH13-063PC was obtained by R/V Helmer Hanssen from a contourite drift west of Lofoten on the 24th of June 2013. See Table 1for further information.

Table 1 Coring location and data of core HH13-063PC

Station	Date	Time (UTC)	Location	Latitude [N] Longitude [E]	Water depth [m]	samples	Recovery [cm]	Comment
HH13-063PC	24.06-13	1132	Lofoten Drift	68.18.612′ 010.29.788′	1131	stored	513	5 sections, upper tube empty, imploded?

3.1 Previous work

The core was retrieved by a piston corer. The piston corer consists of a 12 meters long steel barrel with an inner diameter of 11 cm. The core liner inside the steel barrel has an inner diameter of 10 cm. Weights with a total weight of 2000 kg are attached to the top of the steel barrel.

The core HH13-063PC is 513 cm long. It is noted that the upper tube was empty, probably because it imploded, but according to Tine L. Rasmussen it should not affect the core. The core was divided in 5 sections, capsuled, and stored at 4ºC.

3.1.1 Magnetic Susceptibility

Magnetic susceptibility (MS) measures the sediments ability to magnetize. Variation in mineralogy, concentration and grain size affects the MS.

At deep sea in high latitudes along the path of the North Atlantic Deep Water (NADW) there are high magnetic susceptibility values in sediments deposited from the deep contour currents in the flow path of the overflows from the Nordic seas in interglacial periods (Robinson et al., 1995, Rasmussen et al., 1996, Kissel et al., 1999). During warm periods the bottom currents are strengthened and transport more magnetic material from East Greenland, Iceland and the Faroe islands margin, which gives a higher MS (Kissel, 2005).

Ice rafting was the most important transport method of magnetic terrigenous material to the deep-sea floor during the Pleistocene at high latitudes. The ferrimagnetic IRD are overwriting the bottom current MS signals (Andrews and Tedesco, 1992, Robinson et al., 1995, Jessen et al., 2010). On glaciated margins meltwater plumes (Lekens et al., 2006, Jessen et al., 2010) and mass waste events (Kuijpers et al., 2001) may also alter and overwrite the MS bottom water signal. So, the variation in marine sediments in the arctic may indicate; glacial activity, meltwater plumes, mass transportation, bottom current strength and more (Rasmussen et al., 1996).

The magnetic susceptibility of HH13-063PC was measured on board by a MSCL loop sensor. The measurement was done for every centimetre.

3.2 Laboratory work

Most of the laboratory work was done in the laboratory of the department of geosciences, UiT – The Arctic University of Norway, in Tromsø. Carbon dating was sent to the CHRONO centre at Queens University and the Mg/Ca was sent to Cambridge University.

3.2.1 Splitting the core and logging.

The PVC tube was cut lengthwise by a circular saw. The core was then separated in two halves with an electro osmotic knife. One half was labelled, wrapped and stored for archive in a refrigerator room. The other half was used as the work-part. The surface of the work-part was cleaned by smoothing the surface with plastic cards. The sediment structures were described, and the colours were determined by the Munsell Soil Colour Chart.

3.2.2 X-ray

The work half of the core was run through a GEOTEK MSCL X-ray photography. This is a non-destructive way to get information about the physical properties. X-rays are sent through the core, and different density will give changes in attenuation. Lithology, grain size, water content and compaction are some parameters that alter the density (Migeon et al., 1998) The x-ray image shows darker area as higher density and lighter colour for lower density.

3.2.3 Colour-images

Colour images were taken by an XRF scanner at the institute. Prior to the scanning the core had to be at room temperature overnight for the surface liquid to evaporate, to avoid surface

reflection. The XRF scanner scan the whole length of each section of the core with a resolution below 0.1 mm.

3.2.4 Sediments sampling and sieving

Between 0 and 150 cm of the core, one-centimetre thick slices were taken every tenth centimetre. Samples were taken every fifth centimetre between 150 and 510 cm. There were 88 samples altogether. The samples were weighed and freeze dried. A couple of grams were taken out from the main samples for sortable silt analysis. The samples were wet sieved in 63, 100 and 500 μm fractions. The fractions were dried, weighed and stored in dram glasses. The IRD was counted in the >500 μm fraction and >1 mm fraction. The concentration of IRD grain per sample (no. IRD/gram dry weigh sediment) was calculated.

3.2.5 Radiocarbon dating

Radiocarbon dating is based on the ratio between the unstable isotope ^{14}C and the stable isotopes ^{12}C and ^{13}C. ^{14}C is produced by cosmic rays in the upper atmosphere (Hajdas, 2008). When an organism dies the ^{14}C begins to decay with a half-life of 5730±40 years (Godwin, 1962). The decay has a negative exponential rate, so within 10 half-lives there is only 0,01% radiocarbon left. The most accurate dating is within the five first half lives, making out the last 50,000-55,000 years (Hajdas, 2008). For historical reasons, the conventional way is to use the half-life of 5568 years, which results in a 3% error off the real age, so it needs to be calibrated (Arnold and Libby, 1949, Hajdas, 2008). Radiocarbon dating is founded on the assumptions that all organic and inorganic carbon compounds are in equilibrium with the surroundings, and the invalid assumption that there is a constant ratio of carbon isotopes. This is an invalid assumption because there is a change in the ratio due to change in production rate and in the carbon cycle over time. Consequently, a calibration curve is required. The calibration curve is constantly improved by the international calibration group, IntCal (Hajdas, 2008, Bradley, 2014).

When working with marine material, the marine reservoir effect must be considered. The marine reservoir effect is the age difference between a marine sample and terrestrial sample taken from the same time span (Mangerud et al., 2006). The marine reservoir effect is thought to be changing over time and space with mixing rates of the surface and deep water (Bondevik et al., 2006). For simplicity, modern values for the area based on Mangerud and Gulliksen (1975) was used.(Armstrong and Brasier, 2013)

Four samples with 1200 specimens of *N. pachyderma* were sent to ^{14}CHRONO Centre Queens University in Belfast for dating. The ^{14}C dates were calibrated using Calib 8.2 and the marine calibration curve Marine20 based on Stuiver and Reimer (1993) and Reimer et al. (2020). ΔR is the local variation of the marine reservoir effect. The average ΔR between Troms and Bear Island is calculated from Calib Rev 8.2 based on Mangerud and Gulliksen (1975), and is ΔR = -96 ±37. The calibration was limited within the 1σ range.

3.3 Stable Isotope analysis

$\delta^{18}O$ is the stable oxygen ratio $^{18}O/^{16}O$ and is a standard tool in palaeoceanography. The oxygen isotope in foraminiferal calcite, calcium carbonate ($CaCO_3$), is a function of calcification temperature and sea water $\delta^{18}O$ (Emiliani, 1966, Wefer and Berger, 1991, Bradley, 2014).The $\delta^{18}O$ values of planktic and benthic foraminifera have been mapped throughout the world (Shackleton, 1977). A global signal was found where oxygen isotopes are sensitive to the global ice volume (Mix, 1987). The synchronous variability have been utilized to develop an oxygen isotope stratigraphy (Pisias et al., 1984, Prell et al., 1986, Lisiecki and Raymo, 2005) , making it possibly to date a core based on its $\delta^{18}O$ values.

The carbon isotope ratio, $\delta^{13}C$ ($^{13}C/^{12}C$), can be used to reconstruct changes in paleoproductivity and water ventilation (Jansen, 1989). It is used for tracing water masses, where e.g. North Atlantic Intermediate water has a higher $\delta^{13}C$ value than fresh meltwater (Rørvik et al., 2013)

Oxygen and carbon isotopes were measured in good quality specimens of *Neogloboquadrina pachyderma* (100-500 μm size fraction). Circa 15 specimens with transparent tests and four chambers were picked for each sample. The samples were analysed on a Thermo Scientific MAT253 IRMS + Gasbench II at CAGE – Centre for Arctic Gas Hydrate, Environment and Climate located at UiT – The Arctic University of Norway, in Tromsø, Norway. 82 samples were analysed. One sample at 0 cm was uncertain since the sample was too small.

3.4 Sortable silt

Grain size distribution acts as a physical proxy of bottom current speed as sorting during deposition of the sediment is dependent on flow strength. Sortable silt is the coarsest silt fraction with grain size between 10-63 μm. This size fraction is above the limit of aggregation and is proposed to be the most useful grain-size range to reconstruct current speed. A direct indication of the current speed is the mean size of the sortable silt, $\overline{SS}$. The optimal conditions to use $\overline{SS}$ as a proxy is a constant current with a constant direction (McCave et al., 1995, Hass, 2002, Praetorius et al., 2008), which make contourite drifts an excellent candidate for the sortable silt method.

Ice-rafted detritus (IRD) are sand sized mineral (>63 μm) grains found in deep-ocean sediments. IRD are brought to the deep sea by ice sheets or icebergs (Ruddiman, 1977). If the sand is transported by ice and the silt is transported by bottom currents, there should not be any correlation between them (Hass, 2002). By plotting the $\overline{SS}$ and the sand (wt%) together, a regression line will show the correlation. If there is a positive correlation, it means that the increasing sand/IRD content causes the silt to coarsen. And the closer the correlation coefficient, R^2, is to 1, the stronger the influence of ice rafting.

If the samples are highly influenced by ice rafting, a method by Hass (2002) to reduce the influence of IRD can be used. The method uses the regression equation that was found by plotting IRD against the $\overline{SS}$. The regression equation gives the potential sortable silt, SS_{pot}, which describes the $\overline{SS}$ if there were no current speed fluctuation (R^2=1). The SS_{pot} is then used in the equation $\Delta SS = \overline{SS} - SS_{pot}$ to give the IRD corrected parameter ΔSS. ΔSS shows the relative current speed fluctuations.

For the sortable silt analysis approximately 2 grams of sediments were sampled from the 88 freeze-dried sediments samples. The samples were put in test tubes and added HCl overnight to remove calcareous residues. The next day the samples were washed three times by adding distilled water and centrifuged. To remove organic matter the samples were treated with 20% hydrogen peroxide and put in a hot water bath for 2 hours. There were small amounts of organic matters in the samples since there was none or little reaction in the hydrogen peroxide treatment. The samples were washed and dried. The dried samples were added 20 ml water and put in a shaker machine overnight. Before analysis, Calgon soap was added to avoid the

sediment to agglomerate and put in an ultrasonic bath. The samples were analysed with a LS13320 Laser Diffraction Particle Size Analyzer. Each sample was analysed three times. If the three results were similar the result was saved, if not, they were run again. Of 88 samples two samples needed to be rerun.

The mean sortable silt size, $\overline{SS}$, was calculated geometrically on the metric scale according to the methods of moments using the GRADISTAT software (Blott and Pye, 2001).

3.5 Mg/Ca

Planktonic foraminiferal Mg/Ca thermometry is a well-used method for reconstruction of sea surface temperatures. Mg^{2+} substitutes Ca during growth when temperature increases, so the Mg/Ca ratio increases when the temperatures increases (Chave, 1954, Duckworth, 1977)..

For the Mg/Ca analysis 50-55 specimen of benthic foraminifera *C. neoteri*s (size fraction 150-250 um) were picked. The samples were picked roughly every tenth centimetre between 40-450 cm of the core, depending on the amount and quality. A total of 45 samples were picked and sent to the University of Cambridge for analysis using inductively coupled plasma–optical emission spectrophotometer (ICP-OES). The samples were crushed between two glass slides prior to cleaning. The samples were cleaned by clay removal, reductive cleaning of oxidant coatings, oxidation of organic matter and weak acid leach.

The values were converted to temperatures by species specific calibration method by Kristjánsdóttir et al. (2007) for cold end temperatures for arctic species. Where T is temperature.

(C. neoteretis = 0.864 ± 0.07 * exp(0.082 ± 0.020 * T), r2 = 0.90, SE = ±0.62C)

$$T = \frac{\ln(Mg/Ca) - \ln(0.864)}{0.082}$$

Based on repeated measurements of an in-house standard solution with 1.46 mmol/mol of Mg/Ca at a Calcium concentration of 20 ppm, the analytical error is ±0.017 mmol/mol, equivalent to 0.18 °C using Kristjánsdóttir et al. (2007) calibration. The calibration error for Mg/Ca-BWT calibration is ±0.62°C (Kristjánsdóttir et al., 2007). The combined error and calibration error is therefore circa 0.7°C.

4 Results and interpretation

4.1 Radiocarbon dating, calibration, and sedimentation rates

Table 2 Table of radiocarbon dates

Lab Code	Core	Depth (cm)	Dated material	^{14}C Age BP	1σ cal. Age	Linear sed. Rate (cm/ka)
UBA-41743	HH13-063PC	40	*N.pachyderma*	15246 ± 70	17770 ± 163	-
UBA-41744	HH13-063PC	190	*N.pachyderma*	16568 ± 88	19210 ± 161	104.4
UBA-41745	HH13-063PC	265	*N.pachyderma*	17201 ± 82	20000 ± 160	95.3
UBA-41746	HH13-063PC	390	*N.pachyderma*	19501 ± 104	22860 ± 267	43.7

The four radiocarbon dates were calibrated, and the linear sediment rates were calculated in Table 2. The linear sediment rate is calculated by assuming a constant sedimentation rate between the radiocarbon dates. This is a simple fit since linear interpolation is not taking into consideration that the sedimentation rate is not linear in nature, especially in the transition between glaciomarine and marine sedimentation.

The sedimentation rate from the first radiocarbon date at 390 cm to the next at 265 cm (22.9 to 20 cal. ka BP) gives a sedimentation rate of 43.7 cm/ka. The sediment rate more than doubles from 265 to 40 cm (20 to 17.8 cal. ka BP) with c. 100 cm/ka. The top of the core is probably of Holocene age, so there is a hiatus near the core top.

4.1 Grain size distribution

The sortable silt analysis was used to find the grain size distribution of clay and silt. Results from the sieving process were used for grain sizes above the silt fraction (>63 μm).

The sortable silt analysis (a) in Figure 10) shows a stable clay content of 20 % throughout the core. The silt content is between 70 and 75 %, with several troughs down to 65% between 170 and 420 cm. The >63 μm content of 90-95%, in the >63 μm fraction in b) in Figure 10 is very similar to the silt fraction in the sortable silt analysis. The only different is the minimums at the top and bottom of the core. At the top of the core the minimum >63 μm content is 75%. At the bottom the average <63 μm content is around 65-70%.

The 63-100 μm fraction (c) in Figure 10) has a slightly smaller content than the 100-500 μm fraction (d) Figure 10). The two fractions have partly the same excursions and magnitude. The grain fraction 63-100 μm and 100-500 μm are correlating more than the grain fraction 500 μm correlates with 100-500 μm. The grain fraction 500 μm (in e) in Figure 10) are considered IRD from icebergs. When the grain fraction 100-500 μm follows the pattern of 500 μm it suggests that it is ice rafted (Nam et al., 1995). Since the 100-500 μm fractions correlates more with the previous fraction it is hard to see how much IRD affected it is.

The sortable silt could have been used for the full range of grain sizes, but based on the comparison of the <63 μm range for both methods in fig. a) and b) they almost have the same number of excursion, but not in the same magnitude. The sortable silt analysis seems to underestimate the percentage of the coarsest material at the top and bottom of the core (fig.). This could be due to the samples were taken with a spoon from a plastic bag. The coarsest material could be in the bottom and in the corner of the plastic bag and would not be scooted into the spoon

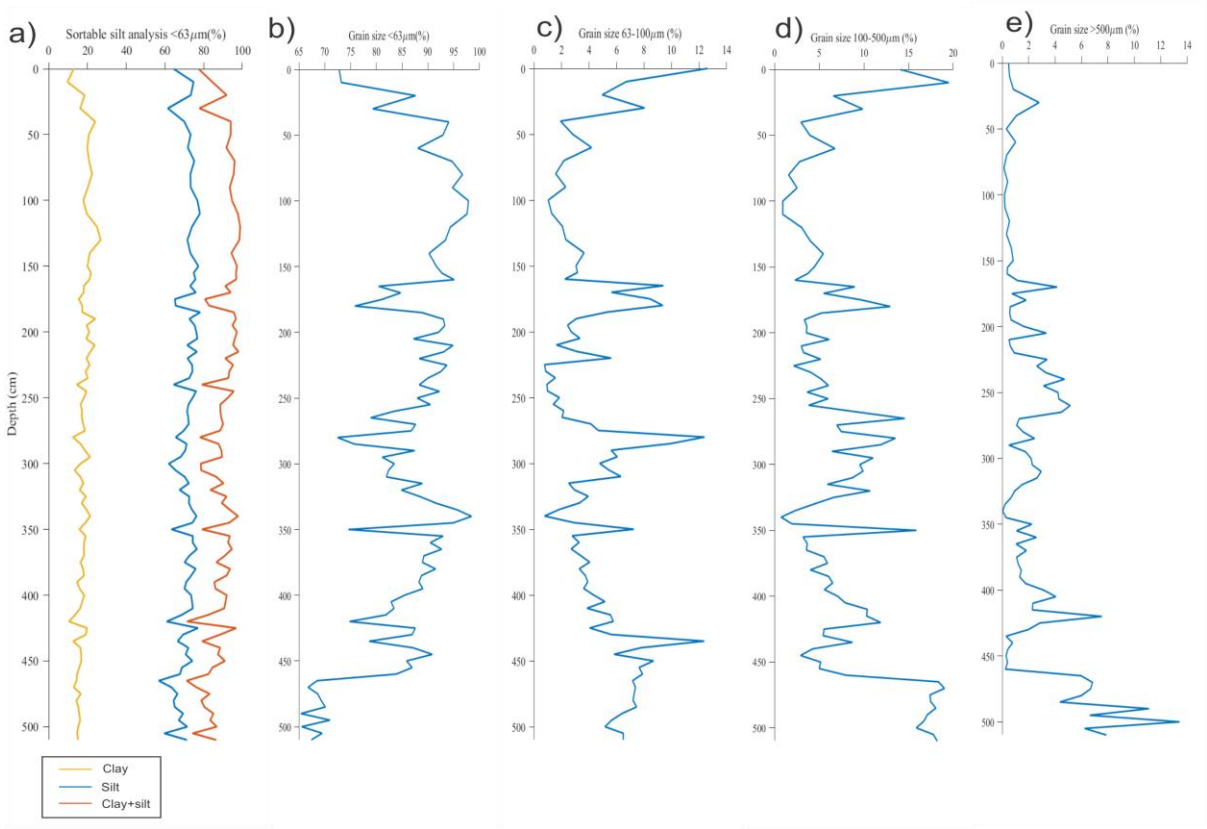

Figure 10 Grain size distribution a) based on sortable silt analysis for the smallest fraction, clay and silt. b), c), d) and e) are from the sieving process and showing the distribution of <63 µm, 63-100 µm, 100-500 µm and >500 µm

4.2 Sortable silt

As seen in Figure 11, the sand content in the core varies between 1.1 and 28.8 % and is on average above 10%. The silt content ranges between 56.8 and 78.2 % while the clay content is between 9.7 and 26.8 %. There is a reduction in the sand content between 40 to 170 cm where it ranges between 1.1 and 8.85%.

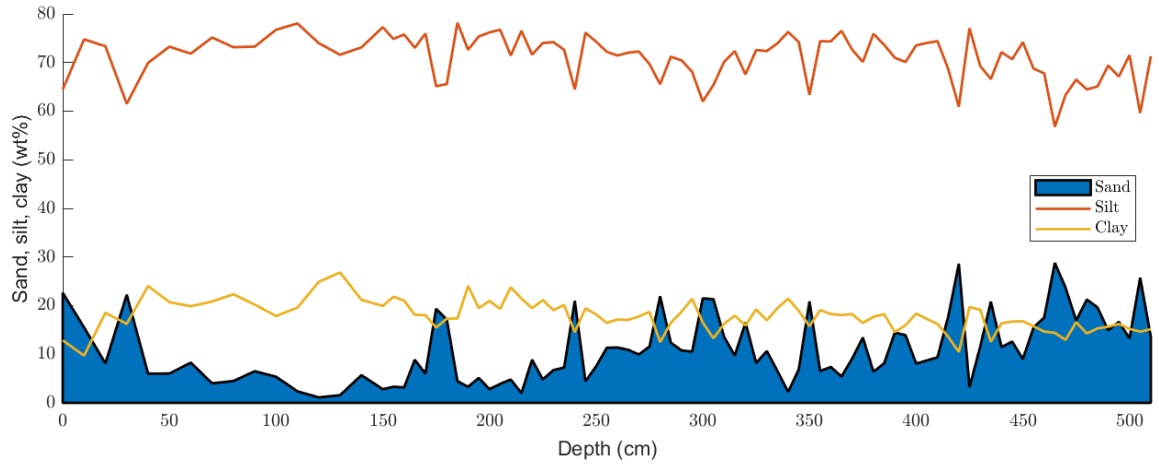

Figure 11 Bulk clay, silt and sand distribution of core HH13-063PC

The regression analysis (Figure 12) between wt% sand and the mean sortable silt, $\overline{SS}$, shows a positive correlation with R^2= 0.87. This indicates a strong influence of ice rafting on the grain size of the sediments and on the SS.

McCave and Hall (2006) argues that the calibration should only be used when there is intense ice rafting. With an average

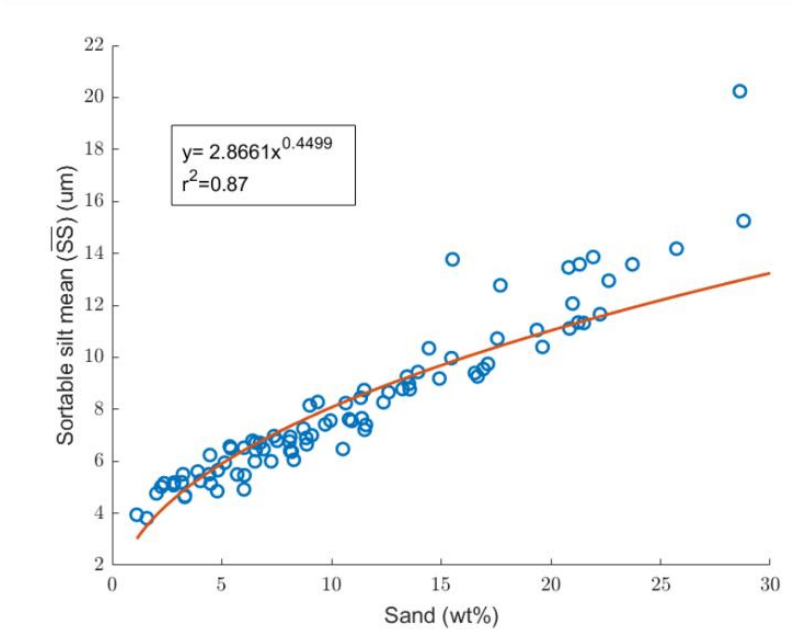

Figure 12 Sand/$\overline{SS}$ relationship

sand content above 10 % and up to 28.8%, an IRD correction is performed with the method of Hass (2002).

Figure 13 shows the transformation from the uncorrected silt graph, $\overline{SS}$, (Figure 13 b) to the IRD corrected silt curve, ΔSS, (Figure 13 d) based on the method of Hass (2002).

The IRD corrected silt curve has contracted several of peaks between 150 and 250 cm which were higher in $\overline{SS}$. On the other hand, a peak at 420 cm has increased in ΔSS. And the ΔSS curve have generally increased from 95 to 140 cm compared to how it was in $\overline{SS}$.

In general, in seems like a relatively stable current conditions from 100 to 400 cm, with a couple of high peaks around 300 cm. At 420 cm it is a short-term event which gives high current speed.

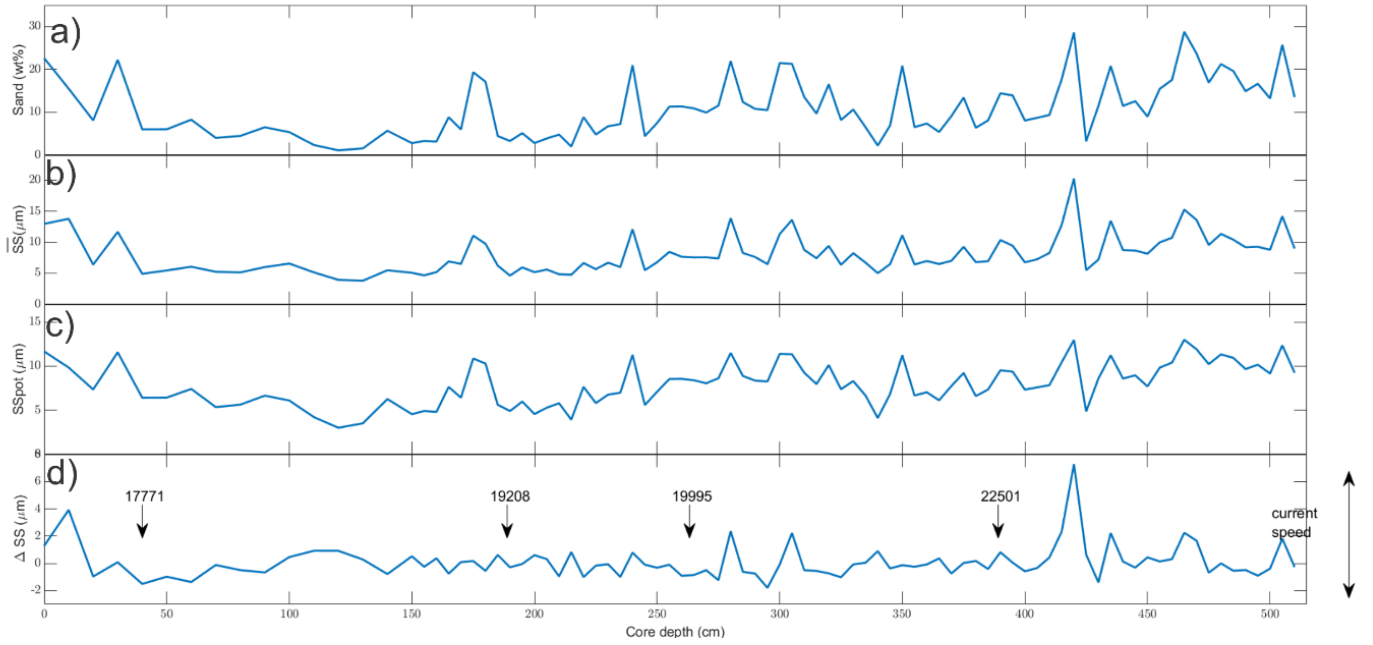

Figure 13 Transformation of the silt mean grain size. a) bulk sand distribution, b) $\overline{SS}$, the mean grain size of the sortable silt, c) $\overline{SS}pot$, the potentially ice rafted silt d) ΔSS ($\overline{SS}$- $\overline{SS}pot$), the current-sorted fraction of the sortable silt mean grain size which can be translated to current speed

4.3 Foraminifera

A description of the complete faunal assemblage for the whole core was not done. The species described are the Atlantic benthic foraminiferal species. *Sigmoilopsis schlumbergeri, Eggerella bradyi, Bulimina costata* and *Cibicidoides aff. Floridanus* were found at 30 and 40 cm. In Figure 17 between 200 cm and the bottom of the core the abundance of planktic and benthic foraminifera (no/g) show the same trends. Between 60 and 200 cm the planktic foraminifera are almost absent, while the benthic are presence with three peaks at 50, 125 and 160 cm with circa 100 no/g. The highest abundance of planktic and benthic foraminifera are generally between 240 and 420 cm with several trough with less foraminifera. The foraminifera flux in Figure 14 shows the same high general flux between 240 and 420 cm with some troughs, e.g. at 310 and 360 cm. Between 240 and 270 there are two large peaks in the planktic and benthic foraminifera flux. There is also a small foraminiferal flux between 60 and 200 cm.

The foraminifera from 460 cm to the bottom, are broken and filled with sediments. This indicates transportation. The Atlantic species found between 30 and 40 cm prefer relative warm temperatures above 3.5 °C and are not found in water temperatures below 2°C (Rasmussen et al., 2003, Rasmussen and Thomsen, 2004). The interval also lacks planktic foraminifera, which may indicate low surface salinity. (Rørvik et al., 2013). The Atlantic species together with the low surface salinity can be correlated to Heinrich Event. Heinrich event can be pinpointed from 30 to 40 cm in HH13-063PC

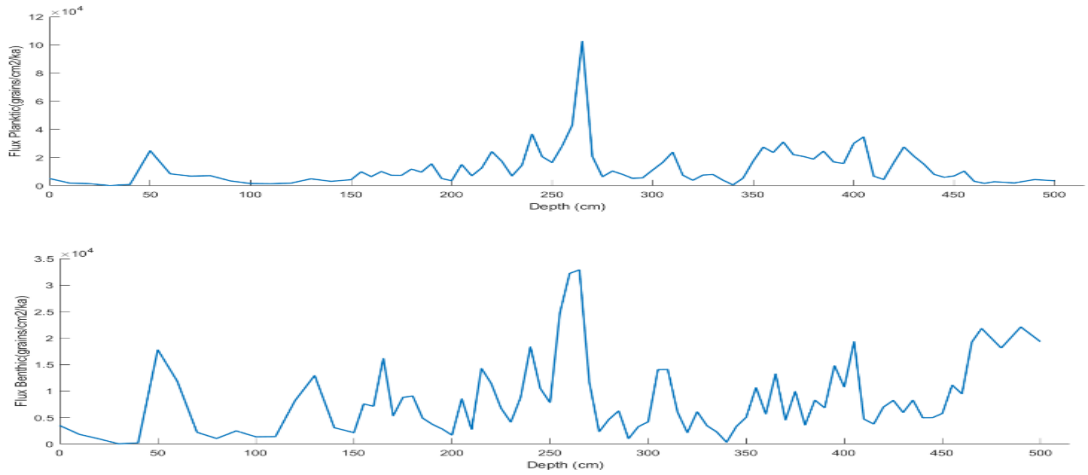

Figure 14: Graphs of foraminiferal fluxes (no.foraminifera/cm^2/ka). The planktic foraminiferal flux at top and benthic foraminiferal flux at the bottom.

4.4 IRD

The IRD distribution in Figure 15 (grain size above 500 μm in blue) and Figure 17 shows little amounts of IRD between the top of the core and 160 cm, except from the peak during the Heinrich event at 30 and 40 cm. From 160 to 360 cm the IRD are fluctuating between 6 and 25 no/g. Except from two troughs at 225 and 335-345 cm with less than 2 no/g. Between 440 and 460 cm there is a period with almost no IRD.

The period between 440 and 460 cm with low IRD and dating at 390 cm to 22.9 cal. ka BP corresponds locally to the Greenland Interstadial 2 or locally the Andøya Interstadial which are dated ca 23.5 cal. ka BP (Vorren and Plassen, 2002, Rørvik et al., 2010). Vorren et al. (2015) found a corresponding between the low IRD in the Lofoten drift and Andøya Interstadial. The high number of IRD below 460 am could be due to a glacigenic debris flow.

4.5 Lithofacies of core HH13-063PC

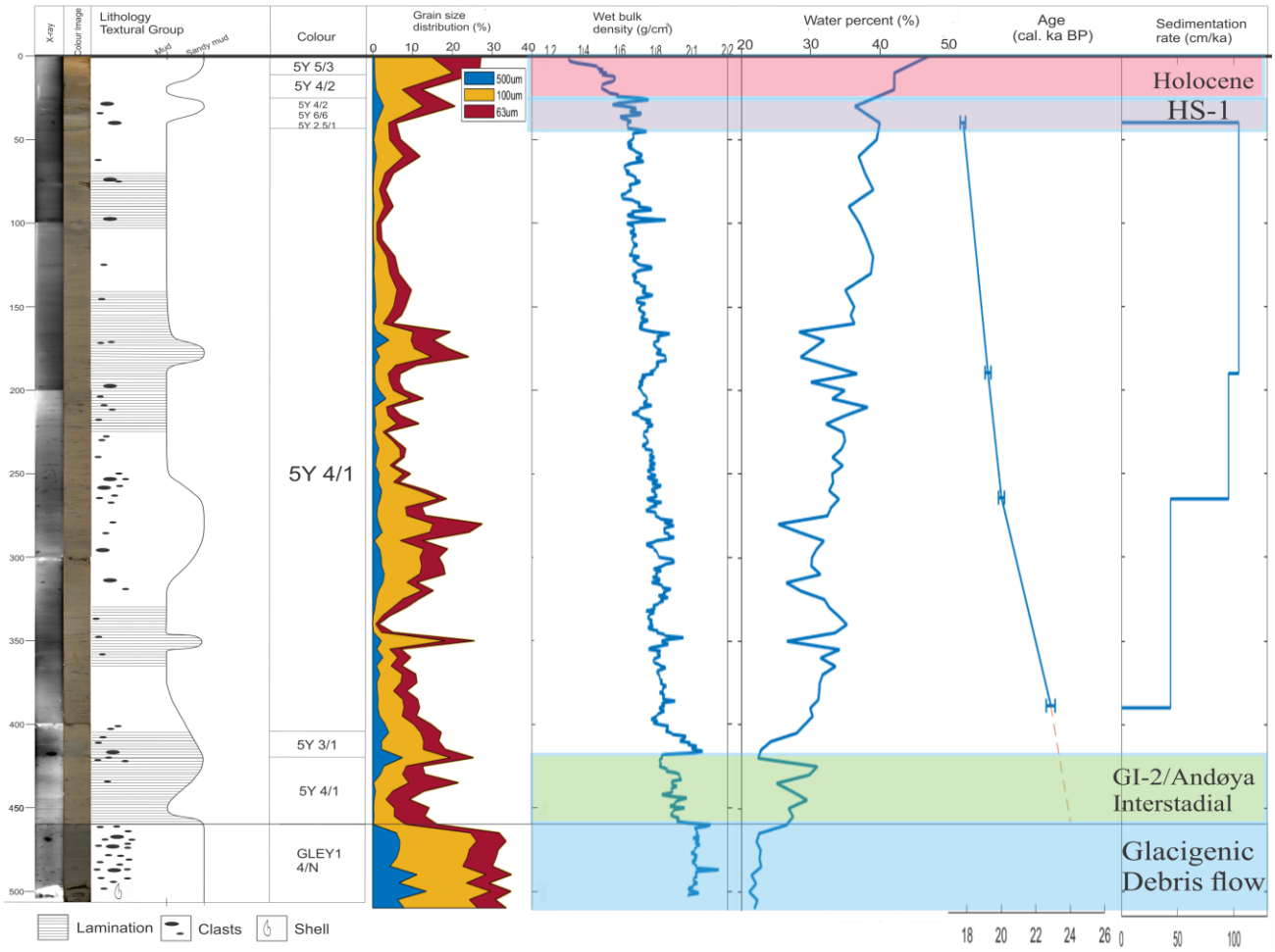

Figure 15 Lithology and physical properties in HH13-063PC. X-ray, colour image, colour, grain size distribution, wet bulk density, water content, age-depth model and sedimentation rate are represented in that order. The events in colours are interpreted from different proxies described in the text.

The core has been subdivided into four main lithofacies and subdivided based on different physical properties within the facies.

Multicoloured mud and sandy mud (facies 1a)

The top 12 cm of the core is olive (5Y 5/3) coloured sandy mud. Between 12 and 30 cm it is olive grey (5Y 4/2) coloured mud.

This sandy mud cap is similar to Laberg and Vorren (2004), the facies is distributed widely throughout the Norwegian Sea and is of Holocene age (Holtedahl, 1959, Damuth, 1978, Henrich et al., 1989) The facies is sediments deposited in oxygenated water by along slope flowing intermediate currents (Laberg and Vorren, 2004).

Multicoloured sandy mud with clasts (facies 1b)

Facies 1b is multicoloured sandy mud with clasts. The colour ranges from olive grey, olive yellow and black (5Y 4/2, 5Y 6/6, and 5Y 2.5/1). Based on the Atlantic foraminifera assemblage this facies is tied to Heinrich stadial 1.

Dark grey mud with clasts (facies 2a)

Facies 2a is homogenous dark grey (5Y-4/1) mud with a low clast content. The facies is partly fainted laminated in some intervals especially in transition to the laminated facies. Facies 2a is found in three intervals: 40-72,105-140 and between 360 and 409 cm.

The homogenous character may indicate a uniform depositional environment, the faint lamination may indicate small disturbances. It is most likely contourite deposited, with some glacimarine influence. The facies is similar to previous studied facies in the area and therefore in agreement with Rørvik et al. (2010), Laberg and Vorren (2004) and Baeten et al. (2014).

Dark grey sandy mud with high clast content (facies 2b)

Facies 2b is a dark grey (5Y-4/1) sandy mud with a high clast content. It has gradual boundaries. Facies 2b is coarser than facies 2a. At its most coarse it has a lower water content (Figure 15). The sedimentation rate is halved from at 95 to 43 cm/ka within the facies. There are some faint laminations.

Baeten et al. (2014) consider this facies to have the same origin as facies 2a. With its coarser content it is believed to be deposited during more glacimarine conditions than facies 2a. The coarse material with high IRD content with large drop stones may indicate calving and maybe some debris release.

Dark grey laminated mud with some few big clasts (facies 3a)

Facies 3a is from 72 to 105 cm. It consists of 95 % mud. There are some big clasts visible at the x-ray. The clasts are circa 1x1.5 cm. The linear sedimentation rate is 104 cm/ka.

Lamination is thought to be from variation in current strengths and more unstable periods (Laberg and Vorren, 2004). The fine-grained sediments with some big clasts may indicate contouritic deposits with disturbance in the current with drop stones from icebergs.

Dark grey laminated mud with clasts (facies 3b)

Facies 3b is between 421 and 460. It is dark grey (5Y-4/1). The mud content is 85 %. There are nearly no IRD. Increasing amount of planktic foraminifera. This is was found to be GI-2 or locally the Andøya Interstadial.

Very dark grey laminated sandy mud with clasts (plumite)

The facies is a very dark grey (5Y-3/1) laminated sandy mud with sharp boundaries (Figure 16). It has a high wet bulk density and low water content (Figure 15). The deposit have the same characteristic as in Baeten et al. (2014), dark colour, high wet bulk density and low water content. There are other intervals with the same properties in facies 3b, but there is a large peak in current speed (ΔSS) and trough in abundance of planktic and benthic foraminifera and a colour change.

This facies is interpreted to be deposited from meltwater plumes as a plumites. Baeten et al. (2014) found two plumites bed dated to 22.2 and 25.5 cal. ka BP. This plumite in HH13-063PC is above the Andøya interstadial (23.5 cal. ka BP) it is possible this is the same plumite bed from 22.2 cal. ka BP which most likely is meltwater derived from Trænadjupet ice stream (Rørvik et al., 2010)

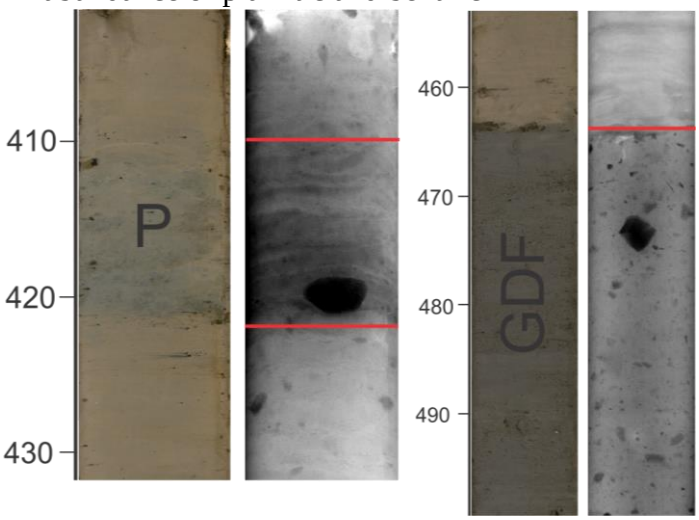

Figure 16 Close up of plumite (P) and facies 4 (Glacigenic Debris Flow)

Dark grey compact sandy mud with high clast content (facies 4)

Dark grey (GLEY 1 4/N) sandy mud with very high clast content occurs at the base of the core. The upper boundary is sharp (Figure 16). There is a large broken shell in the facies and sediment filled and broken foraminifera. The wet bulk density is highest within the core and water content is the lowest.

Baeten et al. (2014) interpret the facies to be a glaciogenic debris flow deposit.

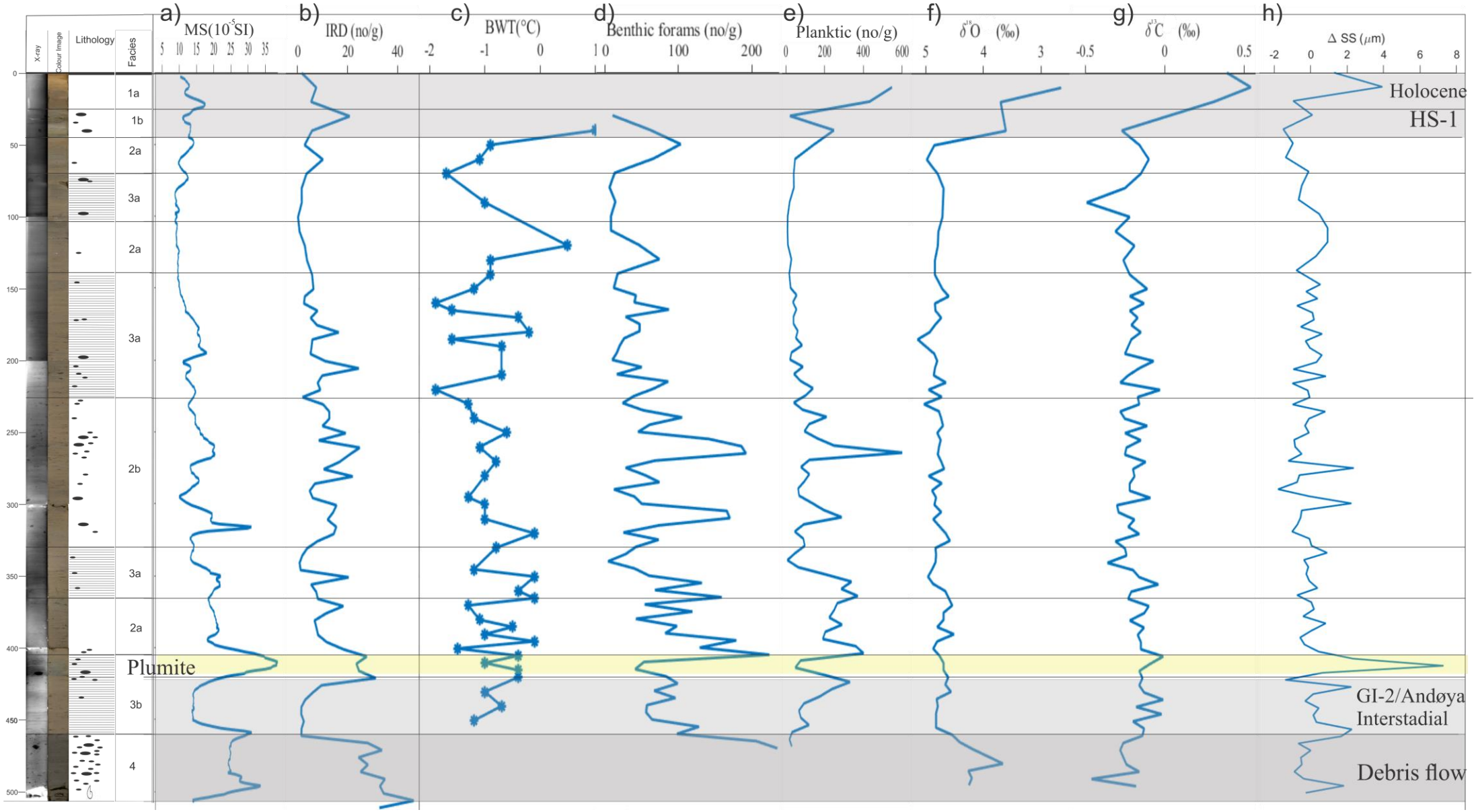

Figure 17 Graph results where a) is Magnetic susceptibility, b) Ice-rafted detritus c) Bottom water temperature, d) Abundance of Benthic foraminifera (no/g) e) Abundance of Planktic foraminifera (no/g) f) stable oxygen isotope ratio g) stable carbon isotope ratio g) ΔSS,IRD corrected mean sortable silt graph which indicate the current strength where higher values is stronger currents. Yellow is a plumite. The grey are events and a debris flow in the bottom of the core.

4.6 Bottom water temperature and stable isotopes

The bottom water temperature (BWT) are measured from 40 to 450 cm. The BWT is overall cold and stable and varies between -1.9 and -0.2 °C. The temperature only exceeds 0 °C two times at 40 and 120 cm with 1 and 0.5 °C. The average temperature is -0.9 °C.

The oxygen isotope values are stable most of the core, except from above 60 cm where the $\delta^{18}O$ are sinking steeply to 3.7-3.6 ‰ at 30 and 40 cm and continues out of range of the graph in Figure 17 to 2.29 ‰ at 0 cm. The $\delta^{18}O$ between 70 and 450 cm are around 4.8‰.

The $\delta^{13}C$ value is very high in Holocene, which make the fluctuation below seems small in Figure 17, the fluctuations are better viewed and explained in the discussion part. There are continuous higher $\delta^{13}C$ values between 345 and 460 cm with an average of -0.14 ‰. Between 100 and 340 the average is -0.21‰. A sudden decrease at 500 cm can be related to debris flow with fresh water following flow from the shelf.

4.7 Magnetic susceptibility

The Magnetic susceptibility is between $10 \cdot 10^{-5}$SI and up to almost $40 \cdot 10^{-5}$SI at the highest peaks. It is in average circa $15 \cdot 10^{-5}$SI. The MS follows the trends of IRD, except from between 180 and 325 cm. Between 240 and 360 cm the MS are following the BWT with the same numbers of excursion, but in a more modest magnitude.

4.8 Summary of the interpretations

- The top 30 cm of the core were dated to Holocene age (11.7 ka BP-) based on the properties of the facies and correlations.
- The interval 30 to 40 cm was dated to Heinrich Event 1 based on the Atlantic benthic foraminiferal species, the increased IRD, the reduced abundance of planktic foraminifera and decreased $\delta^{18}O$ values.

- The interval between 40 and 409 cm will be discussed in the discussion part.
- The interval 409 to 421 cm was labelled a plumite based on the colour change, increased wet bulk density and current speed and decreased water content and abundance of foraminifera.

- The interval 421 to 460 was dated to Greenland Interstadial 2 (GI-2) or Andøya Interstadial (23.5 ka BP), based on the lack of IRD and steadily rising abundance of planktic foraminifera together with the nearby ^{14}C dates (22.9 cal. ka BP at 390 cm).
- The interval 460 to the bottom was interpreted to be a glacigenic debris flow based on the lithology, broken shells and foraminifers, high IRD, high MS, rise in $\delta^{18}O$ values and decrease in $\delta^{13}C$ values.

5 Discussion

5.1 Age Model

The chronology of the core is based on the four calibrated radiocarbon dates. To strengthen the age model, $\delta^{18}O$ and IRD flux were correlated with other studies.

Correlation of IRD flux with Vorren et al. (2015)

Vorren et al. (2015) looks into the glaciation history by combining onshore and offshore dating results from different papers to reconstruct the ice sheets movement during the period 26-16 cal. ka BP. They use onshore carbon dating from lakes and cosmogenic surface exposure dating. The marine deposits are dated by ^{14}C dates on marine calcareous organisms, mainly foraminifera and molluscs. Geological features like moraines and grounding wedge zones were used to correlate the dates to find former locations of the grounding lines of ice streams.

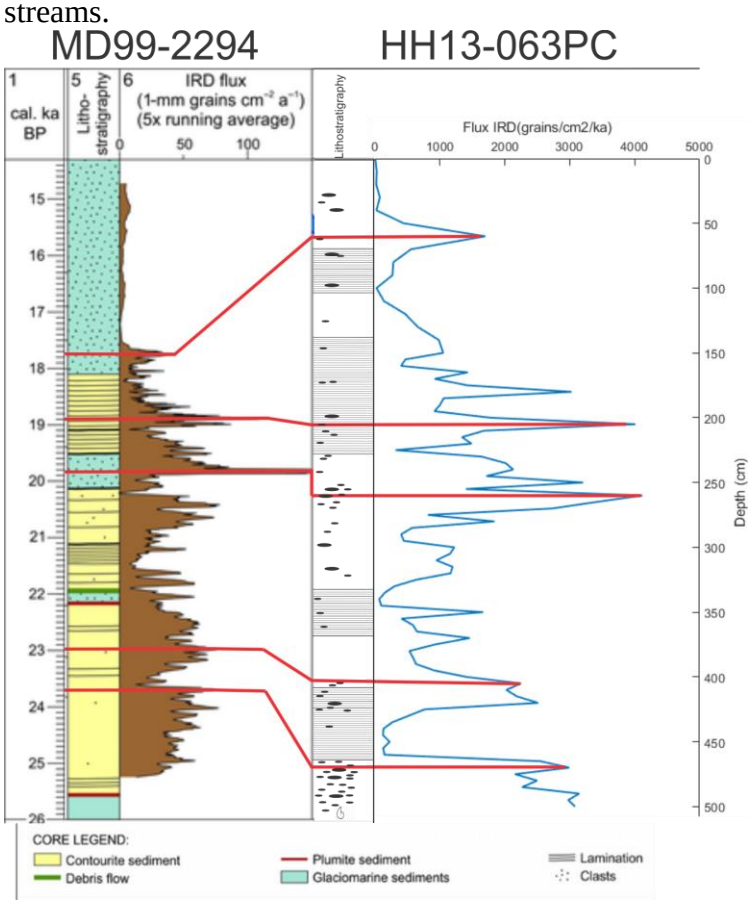

Figure 18 Correlation of lithology and IRD flux. Vorren et al. (2015)

Correlation of $\delta^{18}O$ to Weinelt et al. (2003)

Weinelt et al. (2003) conducted a study in the North Atlantic and Nordic Seas for MIS 2, particularly during the LGM. Five cores were sampled where one core (core 23074) was located in the Nordic Seas southwest of Lofoten, west of Brønnøysund, Nordland. This study was chosen firstly because the good correlation of $\delta^{18}O$ and secondly because ^{14}C dates were given so it was possible to re-calibrate. Their main proxy was $\delta^{18}O$ which was obtained from N. pachyderma sin. The age model of 23074 is based on 15 Accelerator Mass Spectrometry (AMS) ^{14}C dates on monospecific samples of N.pachyderma sin. The ^{14}C dates from core 23074 were calibrated like HH13-063PC by using Calib 8.2 and the marine calibration curve Marine20 based on Stuiver and Reimer (1993) and Reimer et al. (2020) with $\Delta R = -96 \pm 37$ according to Mangerud and Gulliksen (1975). The calibration was limited within the 1σ range.

By close correlation to core 23074 of the $\delta^{18}O$ values of HH13-063PC with the $\delta^{18}O$ values of 23074 it is possible to transfer some of the ^{14}C dates from 23074 to HH13-063PC to strengthen the age model.

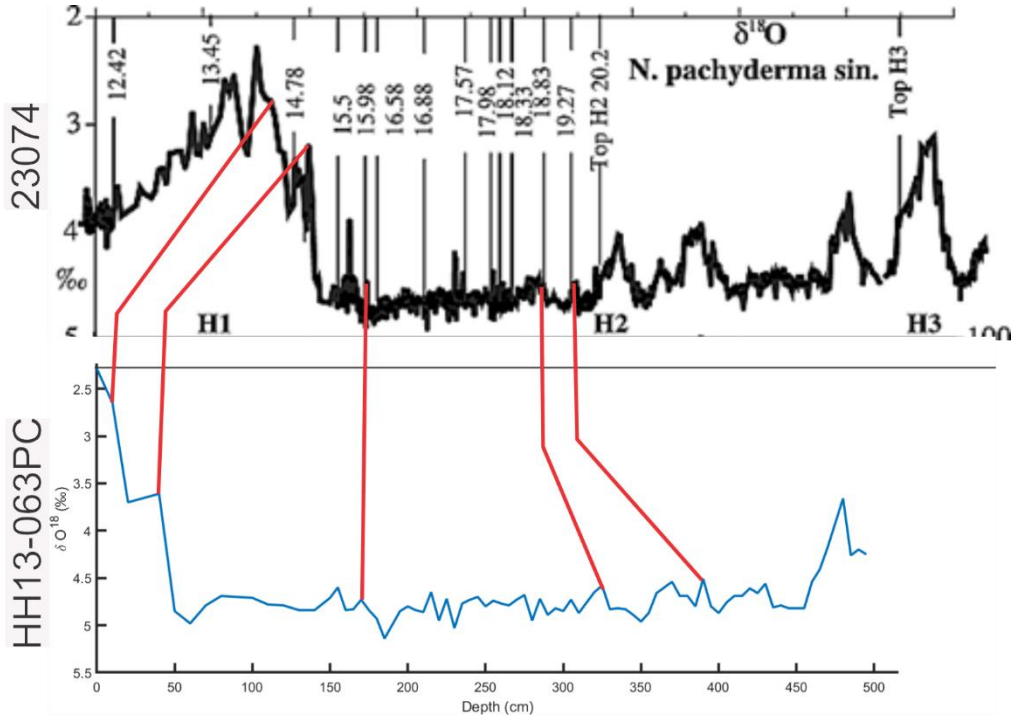

Figure 19 Correlation of $\delta^{18}O$ between HH13-063PC and core 23074 examined by Weinelt et al. (2003).

Age model with rbacon

The obtained dates from ^{14}C dating and correlation are presented in table 3.

Depth (cm)	HH13-069PC	Vorren et al. (2015)	Weinelt et al. (2003)	
	Cal yr BP			^{14}C dates
25			17 170	14780
40	17 770			15250
60		17 750		-
170			18 570	15980
190	19 210			16570
260		19 800		-
265	20 000			17200
325			22 010	18830
385			22 440	19270
390	22 860			19501
405		23 000		-

Bacon is an approach of age-depth modelling. Bacon uses Bayesian statistics that use probability distribution based on prior information. The core is divided into 5 cm sections, where the accumulation rate in each section is calculated through millions of Markov Chain Monte Carlo iterations and only a fraction will be stored (Blaauw and Christen, 2013). The age-depth model starts at 25 cm and is extrapolating to 450 cm, right at the top of the section of the mass waste event deposit.

The result of age depth modelling with no modification is: 100% of the dates overlap with the age-depth model (95% ranges), and the model has a good MCMC iteration. Therefore, the model will not be further modified.

It correlates well except from at the top 40 and 60 cm.

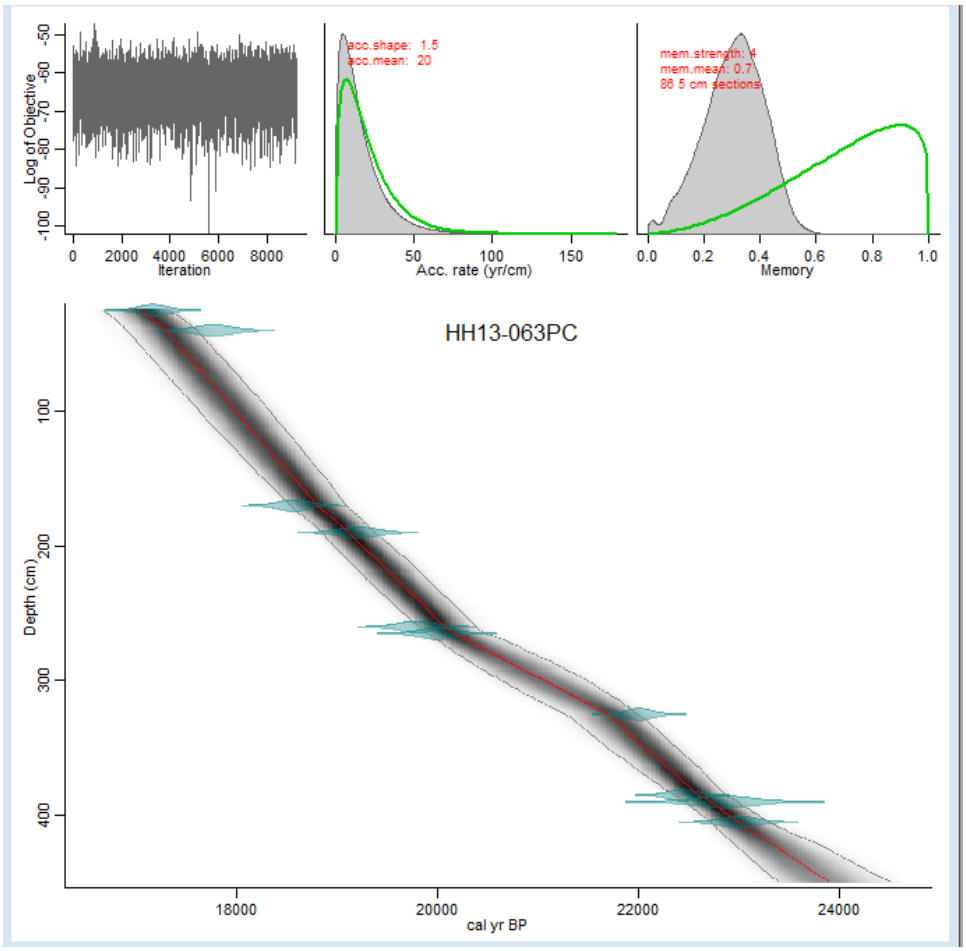

Figure 20 The upper panels show the MCMC iterations (it is considered a good run, because it shows a stationary distribution with little structure among neighbouring iterations). Bottom panel shows the calibrated ^{14}C dates (transparent blue) and the age-depth model (darker grey indicates more likely calendar ages, grey dashed line shows 95% confidence interval, red line is the 'best fitted line'

5.2 Paleoceanography

The interval between 40 and 409 cm will be examined. This is the period between the Andøya interstadial and 17.7 cal. ka BP, close to the start of the Heinrich Event.

Between 100 and 150 cm (see green field in Figure 21) the ΔSS (current speed) and BWT are rising synchronous. The temperature is steadily rising to 0.5 °C and there is a similar rising in the current strength. The interval 100 to150 cm is mainly within facies 2a, homogenous with little IRD. There is a low planktic flux and a high benthic flux. According to the age model in Figure 20 this equals to circa 18.2 to 18 cal. ka BP. There is a warm period from 18.8 to 18.1 cal. ka BP with a mean July air temperature between 0 and 3° (Vorren et al., 2013). The warming can cause excessive ice melting giving fresh surface water that gives a decrease in planktic foraminifera. The fresh surface water gives a stratified water column, where the more saline Atlantic water is isolated and keep its heat beneath the light fresh surface water (Rasmussen et al., 1996, Sessford et al., 2019).

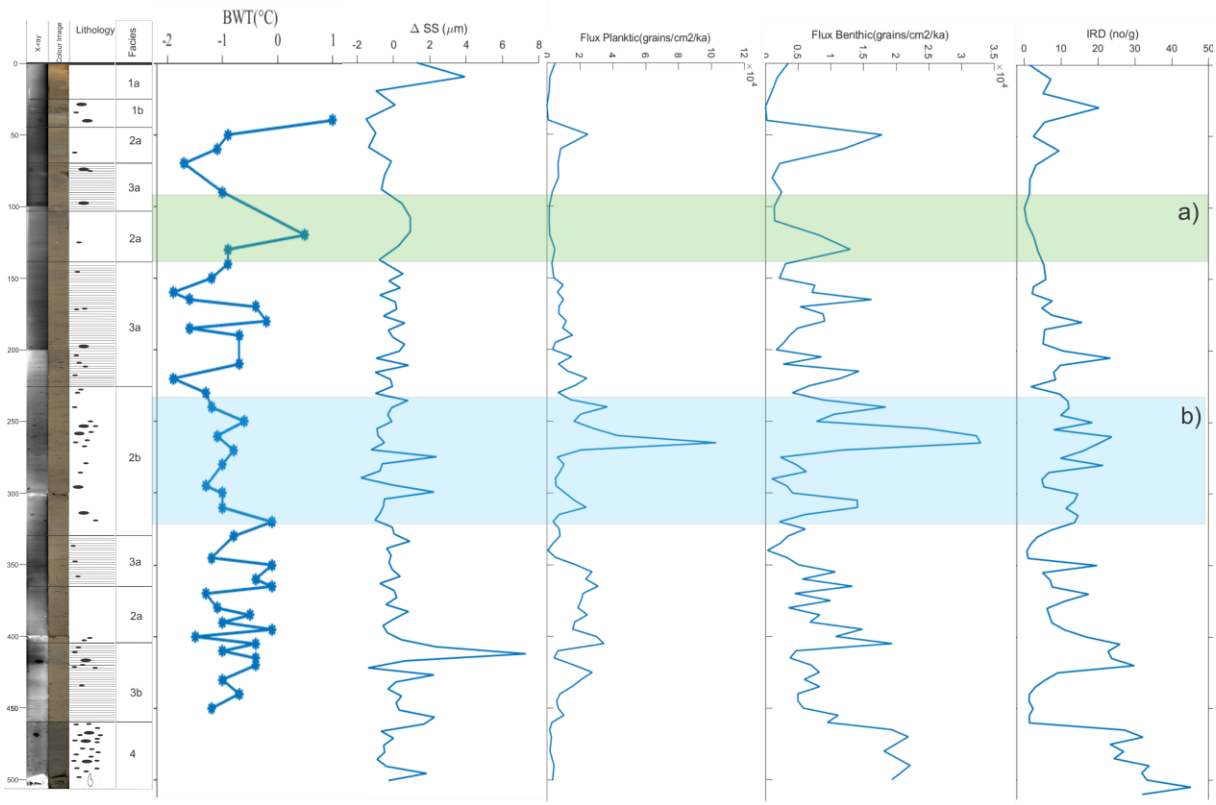

Figure 21 Interpretation of oceanographic environment. The green field has a rise in BWT and current strength. The Blue field shows a rise in planktic and benthic foraminiferal flux which correlates with the current speed, and a continuous cold BWT.

The blue field in Figure 21 is between 230 and 325 cm makes out most of facies 2b. This represents the period circa 20-19.8 cal. ka BP (Figure 20) and is thought to be a cold period with low mean July temperatures (Vorren et al., 2013). Weinelt et al. (2003) finds the minimum SST occurring between 21-20.5 cal. ka BP with rare extremely cold summers that could lead to sea ice along the continental margin. Facies 2b have coarser material, low water content and fainted lamination. Figure 21 shows a maximum of planktic and benthic foraminiferal flux during this period. There is a rise in the current strength simultaneous with the peaks in the foraminiferal flux. The BWT are continuously cold throughout this period. The mean $\delta^{13}C$ are rising at 340 cm that last to 100 cm showing a generally better ventilated water.

The increased bioproductivity together with stronger bottom currents can indicate vertical circulation with upwelling, which gives nutrition to the planktic foraminifera and increased ventilation on the bottom. Together with the cold climate with sea ice along the continental margin it is tempting to suspect coastal polynyas. Polynyas are formed when katabatic winds blow away sea ice and it creates open waters. (Bauch et al., 2001, Knies et al., 2018). The warm nutritious Atlantic water rises to the polynyas which increases the bioproduction. The water cools down beneath the ice and sinks (Bauch et al., 2001). It has been speculated if there have been polynyas in the Nordic Seas that have formed deep water in the Western North Atlantic. The existence and location of those polynyas are not known (Knies et al., 2018, Keigwin and Swift, 2017).

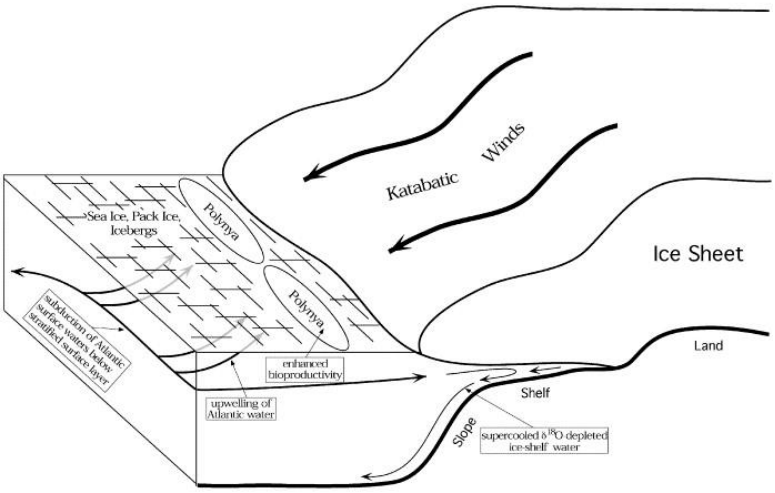

Figure 22 Formation of polynyas and pathways of water masses (Bauch et al., 2001).

Rørvik et al. (2013) examined core MD99-2294, which was retrieved at 1121 meters depth and located 18.5 km south of HH13-063PC. HH13-063PC was retrieved at 1131 meters depth. In Rørvik et al., 2013 is the high δ^{13} values are explained by North Atlantic intermediate water circulation with a warm subsurface temperature. There are two (possibly three, but it is out of the time range here) events where there is a large decrease in the benthic δ^{13} values (see uppermost graph in Figure 24). The depletions are linked to extensive cooling by meltwater released into the Nordic Seas that interrupts the flow of the warm Atlantic surface water. These events are also recorded in north eastern North Atlantic Ocean off Ireland by Peck et al. (2006).

During ice melting and meltwater release of fresh water, the planktic foraminifera tries to avoid the low-salinity condition by changing their depth habitat. This gives different depth distribution of foraminifer under different hydrographic conditions (Carstens et al., 1997). Therefore is it thought that during cold stadials, the planktic foraminifera are at greater depths in the Nordic Seas, where they are in contact with Atlantic water and are recording the relatively warm water below the halocline (Dokken et al., 2013)

In MD99-2294 the planktic and benthic oxygen isotope records almost completely parallel, while the carbon isotope record is to a lesser extent. Therefore, it is a reasonable interpretation that the planktic and benthic foraminifera are in contact with the same intermediate water. The magnitude of the planktic foraminiferal isotopes are smaller than the benthic foraminifera. The parallel relationship of the stable isotope between planktic and benthic is assumed to be valid for HH13-063PC as well. As seen in Figure 24 the event 1 is more visible in core HH13-063PC than event 2. Event 1 is between 70 and 100

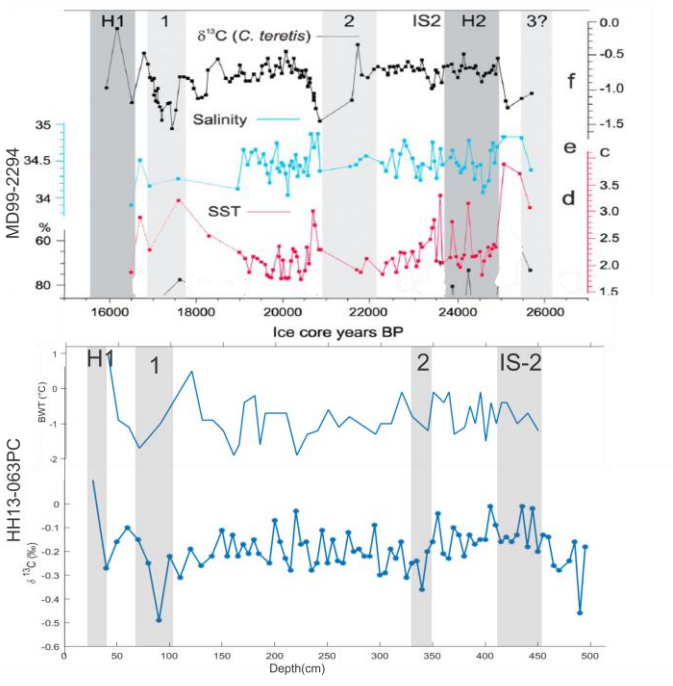

Figure 23 The record of $\delta^{13}C$ of benthic foraminifera and calculated salinity and Sea Surface Temperature in the upper graph of MD99-2294. Event 1 and 2 in MD-2294 are marked in light grey. The same events are marked in the lower graph with and correlated with the planktic $\delta^{13}C$. The BWT is also included in lower graph for HH13-063PC.

cm in core HH 13-063PC which is the uppermost laminated facies 3a. This interval has the finest material of the three facies 3a intervals. This is after or during the warm period (18.8-18.1 ka BP). There is a low bioproductivity and the BWT is decreasing rapidly within the event. Event 2 is around 340 cm in the core and is about 10 cm thick. It is also within the laminated facies 3a. There is also a minimum in BWT, IRD, current speed and in the abundance of foraminifera.

By seeing event 1 and 2, there are several of these events throughout the core HH13-063PC. There are synchronous troughs in the δ^{13} values, BWT, in the abundance of foraminifera, current speed and to a degree in the IRD. The events are mapped in Figure 25 in purple as intermediate water formation. The intermediate water formation events are in the laminated facies 3a. There are a couple of marked intermediate formation events outside the boundary of facies 3a, but the boundaries between the facies are gradual. The temperature and benthic foraminifera abundance are rising between the events. So, the interpretation is that there is a steady state of stratified water mass with cold water on top and warm Atlantic water flowing beneath. This state is interrupted by meltwater supply. The sudden decrease of benthic foraminifera during the meltwater events may be a clue for brine water rejection since brine rejections are corrosive towards benthic foraminifera (Fossile et al., 2020). Brine rejections are usually formed when sea ice grows at the shelf, the salty dense water gets rejected and is transported downslope (Craig and Gordon, 1965, Dokken and Jansen, 1999). Since the site is beneath a canyon, the canyons could be funnelling cold dense water from the shelf over the site.

The generally low BWT in HH13-063PC is considerably closer to the cold modern BWT than the warmer BWT during LGM. The deep Nordic Seas was 1.5 °C warmer during LGM than in Holocene (Ezat et al., 2021). The records of BWT from Svalbard during LGM seems to be generally warmer with several points above 1°C (El Bani Altuna et al., 2020). There is an error of circa 0.7 °C in Mg/Ca and calculation of BWT. It is unknown if the colder temperature is due to an error, a local phenomenon caused by the canyon, the intermediate water, or the deepwater formation.

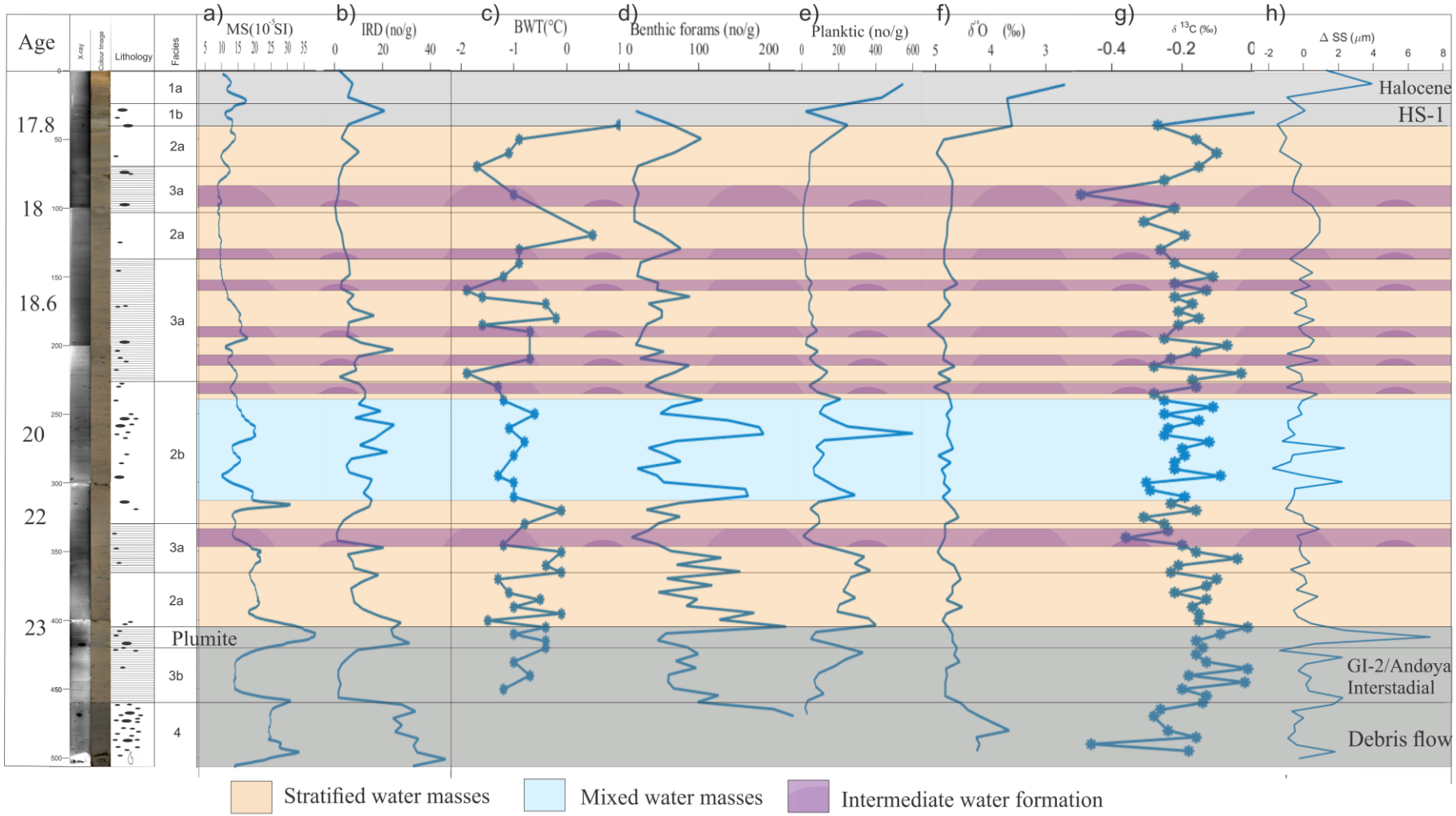

Figure 24 Overview the of water masses during stadial a) is magnetic susceptibility, b) is Ice-rafted debris, c) is Bottom Water Temperature, d) and e) is abundance of benthic and planktic foraminifera, f) and g) is the oxygen and carbon isotope h) is ΔSS shows the current strength where a higher value indicates stronger currents. The orange fields are Stratified water masses with a cold top layer and warmer subsurfacewater. Purple is intermediate water formation. Blue is mixed water masses

5.3 Glaciation

The canyon above the site does not reach the shelf break. The canyon started to develop at the base of the continental slope and had an upslope retrogressive erosion. The canyon terminates below the Lofoten contourite drift (Rise et al., 2013). The canyon was formed before the LGM.

The glacigenic debris flow (GDF) in the bottom of core HH13-063PC beneath the Andøya Interstadial layer is prior to 23.5 cal. ka BP. The neighbouring core MD99-2294 does not have the similar GDF- facies. Core GS10-163PC, retrieved circa 47 km further southeast (Figure 1) described in Baeten et al. (2014), has glacigenic debris flow which is dated between 22 and 21.9 cal. ka BP. So, there is no simultaneous events in the southern direction from core HH13-063PC. Vorren et al. (2015) concludes that the debris flow in Baeten et al. (2014) is a local phenomenon, maybe released due to isostatic adjustment or other mechanisms. As of today, there is no evidence of the ice sheet reaching the shelf break above the site. The GDF at in HH13-063PC may also been released due to isostatic adjustment or by the retrogressive erosion of the canyon above the site.

The mean grain size is coarser in HH13-063PC than in the MD99-2294 and GS10-163PC. The clay content is around 40 % in GS10-163PC and around 50% in MD99-2294. While the clay content in HH13-063PC is stable at 20 %. The large difference of the clay content in such a small area could be explained by the closeness to the canyon. Rise et al. (2013) suggests that ice streams from the troughs distributed sediments and sediment-laden meltwater towards the head of the canyons. The discharge cascaded along the canyon causing erosion and retrogressive failures.

There is a moraine less than 5 km from the shelf break above the site (Figure 3). It may explain how the sediments are more glacimarine influenced than the neighbouring cores with coarser material and longer interval of laminated materials due to brine rejection or other glacial processes. This site is closer to the end moraine of the Egga I and Egga II events than the other cores.

6 Conclusion

Core HH13-063PC from the Lofoten Contourite Drift west of the Lofoten Islands has been analysed to reconstruct the paleoceanography during the Last Glacial Maximum.

- The core has coarser sediments than two other cores from the Lofoten drift, described in Laberg and Vorren (2004) and Baeten et al. (2014). This is thought to be either because it was closer to the ice sheets with more glacial processes or because core site of HH13-063PC was located beneath a canyon.
- There is no evidence of the ice sheet reaching the shelf break during LGM. There is a glacigenic debris flow at the bottom of the core dated older than 23.5 cal. ka BP. This glacigenic debris flow is thought to be deposited due to isostatic adjustment or through the canyon.
- The top of the core is dated to Holocene. The Heinrich Event 1 is recognised between 30 and 40 cm. There is a hiatus between the layers.
- The oceanographic conditions between the Heinrich Stadial (40 cm that ^{14}C- dated to 17.7 cal. ka BP) and Andøya Interstadial (23.5 cal. ka BP) had two states. The main state was stratified water masses with a cold, light meltwater on the surface and warm Atlantic water beneath. The other state was between 20 and 19.8 cal. ka BP the water masses were mixed with high bioactivity. The suspicion is polynyas with upwelling of Atlantic Water causing the mixed water and the higher bioproductivity.
- The stratified water masses were interrupted by cold, sinking water. This was most likely brine rejections, that flushed cold, dense salty water along the slope cooling down the bottom water temperature and corroded the benthic foraminifera.
- There is a cold stable BWT throughout the core, which are more similar to modern settings than LGM settings. It may be due to severe intermediate water formation, either in local scale or even maybe deepwater formation.

- Further studies should involve BWT analysis along the shore of Lofoten-Vesterålen to see if this is a local phenomenon. Also, a ^{14}C reservoir ages analysis of benthic foraminifera at this depth and deeper would be interesting to see if it is a site for intermediate or deepwater formation.

REFERANCES

ÁLVAREZ-SOLAS, J., MONTOYA, M., RITZ, C., RAMSTEIN, G., CHARBIT, S., DUMAS, C., NISANCIOGLU, K., DOKKEN, T. & GANOPOLSKI, A. 2011. Heinrich event 1: an example of dynamical ice-sheet reaction to oceanic changes. *Clim. Past,* 7**,** 1297-1306.

ANDREWS, J. & TEDESCO, K. 1992. Detrital carbonate-rich sediments, northwestern Labrador Sea: Implications for ice-sheet dynamics and iceberg rafting (Heinrich) events in the North Atlantic. *Geology,* 20**,** 1087-1090.

ARMSTRONG, H. & BRASIER, M. 2013. *Microfossils,* John Wiley & Sons.

ARNOLD, J. R. & LIBBY, W. F. 1949. Age determinations by radiocarbon content: checks with samples of known age. *Science,* 110**,** 678-680.

BAETEN, N. J., LABERG, J. S., VANNESTE, M., FORSBERG, C. F., KVALSTAD, T. J., FORWICK, M., VORREN, T. O. & HAFLIDASON, H. 2014. Origin of shallow submarine mass movements and their glide planes—Sedimentological and geotechnical analyses from the continental slope off northern Norway. *Journal of Geophysical Research: Earth Surface,* 119**,** 2335-2360.

BAUCH, H. A., ERLENKEUSER, H., SPIELHAGEN, R. F., STRUCK, U., MATTHIESSEN, J., THIEDE, J. & HEINEMEIER, J. 2001. A multiproxy reconstruction of the evolution of deep and surface waters in the subarctic Nordic seas over the last 30,000 yr. *Quaternary Science Reviews,* 20**,** 659-678.

BÉ, A. W. & HUTSON, W. H. 1977. Ecology of planktonic foraminifera and biogeographic patterns of life and fossil assemblages in the Indian Ocean. *Micropaleontology,* 23**,** 369-414.

BLAAUW, M. & CHRISTEN, J. A. 2013. Bacon Manual v2. 3.3.

BLINDHEIM, J. 1990. Arctic intermediate water in the Norwegian Sea. *Deep Sea Research Part A. Oceanographic Research Papers,* 37**,** 1475-1489.

BLINDHEIM, J. 2005. The Nordic Seas, main oceanographic features. *In:* DRANGE, H., DOKKEN, T., FUREVIK, T., RUDIGER, G. & BERGER, W. H. (eds.) *The Nordic Seas: An Intergrated Perspective.* American Geophysical Union.

BLOTT, S. J. & PYE, K. 2001. GRADISTAT: a grain size distribution and statistics package for the analysis of unconsolidated sediments. *Earth surface processes and Landforms,* 26**,** 1237-1248.

BOND, G., BROECKER, W., JOHNSEN, S., MCMANUS, J., LABEYRIE, L., JOUZEL, J. & BONANI, G. 1993. Correlations between climate records from North Atlantic sediments and Greenland ice. *Nature,* 365**,** 143-147.

BONDEVIK, S., MANGERUD, J., BIRKS, H. H., GULLIKSEN, S. & REIMER, P. 2006. Changes in North Atlantic radiocarbon reservoir ages during the Allerød and Younger Dryas. *Science,* 312**,** 1514-1517.

BOYLE, E. A. & KEIGWIN, L. 1987. North Atlantic thermohaline circulation during the past 20,000 years linked to high-latitude surface temperature. *Nature,* 330**,** 35-40.

BRADLEY, R. S. 2014. *Paleoclimatology: Reconstructing Climates of the Quarternary,* Elsevier Inc.

BUHL-MORTENSEN, L., BØE, R., DOLAN, M. F., BUHL-MORTENSEN, P., THORSNES, T., ELVENES, S. & HODNESDAL, H. 2012. Banks, troughs, and

canyons on the continental margin off Lofoten, Vesterålen, and Troms, Norway. *Seafloor Geomorphology as Benthic Habitat.* Elsevier.
CARSTENS, J., HEBBELN, D. & WEFER, G. 1997. Distribution of planktic foraminifera at the ice margin in the Arctic (Fram Strait). *Marine Micropaleontology,* 29**,** 257-269.
CAVALIER-SMITH, T. & CHAO, E. E.-Y. 2003. Phylogeny and classification of phylum Cercozoa (Protozoa). *Protist,* 154**,** 341-358.
CHAVE, K. E. 1954. Aspects of the biogeochemistry of magnesium 1. Calcareous marine organisms. *The Journal of Geology,* 62**,** 266-283.
CLARK, P. U., DYKE, A. S., SHAKUN, J. D., CARLSON, A. E., CLARK, J., WOHLFARTH, B., MITROVICA, J. X., HOSTETLER, S. W. & MCCABE, A. M. 2009. The last glacial maximum. *science,* 325**,** 710-714.
CRAIG, H. & GORDON, L. I. 1965. Stable isotopes in oceanographic studies and paleotemperatures. *V. Lischi e Figli, Pisa,* 122.
CROCKET, K. C., VANCE, D., GUTJAHR, M., FOSTER, G. & RICHARDS, D. 2011. Persistent Nordic deep-water overflow to the glacial North Atlantic. *Geology,* 39**,** 515-518.
DAHLGREN, K. T. & VORREN, T. O. 2003. Sedimentary environment and glacial history during the last 40 ka of the Vøring continental margin, mid-Norway. *Marine Geology,* 193**,** 93-127.
DAHLGREN, K. T., VORREN, T. O. & LABERG, J. S. 2002. Late Quaternary glacial development of the mid-Norwegian margin—65 to 68 N. *Marine and Petroleum Geology,* 19**,** 1089-1113.
DAMUTH, J. E. 1978. Echo character of the Norwegian—Greenland Sea: relationship to Quaternary sedimentation. *Marine Geology,* 28**,** 1-36.
DARLING, K. F., KUCERA, M., KROON, D. & WADE, C. M. 2006. A resolution for the coiling direction paradox in Neogloboquadrina pachyderma. *Paleoceanography,* 21.
DOKKEN, T. M. & HALD, M. 1996. Rapid climatic shifts during isotope stages 2–4 in the Polar North Atlantic. *Geology,* 24**,** 599-602.
DOKKEN, T. M. & JANSEN, E. 1999. Rapid changes in the mechanism of ocean convection during the last glacial period. *Nature,* 401**,** 458-461.
DOKKEN, T. M., NISANCIOGLU, K. H., LI, C., BATTISTI, D. S. & KISSEL, C. 2013. Dansgaard‐Oeschger cycles: Interactions between ocean and sea ice intrinsic to the Nordic seas. *Paleoceanography,* 28**,** 491-502.
DOWDESWELL, J. A. & DOWDESWELL, E. K. 1989. Debris in icebergs and rates of glaci-marine sedimentation: observations from Spitsbergen and a simple model. *The Journal of Geology,* 97**,** 221-231.
DUCKWORTH, D. L. 1977. Magnesium concentration in the tests of the planktonic foraminifer Globorotalia truncatulinoides. *The Journal of Foraminiferal Research,* 7**,** 304-312.
DUPLESSY, J., LABEYRIE, L., JUILLETLECLERC, A., MAITRE, F., DUPRAT, J. & SARNTHEIN, M. 1991. Surface salinity reconstruction of the North-Atlantic ocean during the last glacial maximum. *Oceanologica Acta,* 14**,** 311-324.
DUPLESSY, J., SHACKLETON, N., FAIRBANKS, R., LABEYRIE, L., OPPO, D. & KALLEL, N. 1988. Deepwater source variations during the last climatic cycle and their impact on the global deepwater circulation. *Paleoceanography,* 3**,** 343-360.

EL BANI ALTUNA, N., EZAT, M., GREAVES, M. & RASMUSSEN, T. L. 2020. Millennial‐scale changes in bottom water temperature and water mass exchange through the Fram Strait 79°N, 63–13 ka.

EL BANI ALTUNA, N. E., PIEŃKOWSKI, A. J., EYNAUD, F. & THIESSEN, R. 2018. The morphotypes of Neogloboquadrina pachyderma: Isotopic signature and distribution patterns in the Canadian Arctic Archipelago and adjacent regions. *Marine Micropaleontology,* 142**,** 13-24.

ELDEVIK, T. & NILSEN, J. E. Ø. 2013. The Arctic–Atlantic thermohaline circulation. *Journal of climate,* 26**,** 8698-8705.

EMILIANI, C. 1966. Isotopic paleotemperatures. *Science,* 154**,** 851-857.

ERICSON, D. B. 1959. Coiling direction of Globigerina pachyderma as a climatic index. *Science,* 130**,** 219-220.

EZAT, M. M., RASMUSSEN, T. L. & GROENEVELD, J. 2014. Persistent intermediate water warming during cold stadials in the southeastern Nordic seas during the past 65 ky. *Geology,* 42**,** 663-666.

EZAT, M. M., RASMUSSEN, T. L., HAIN, M. P., GREAVES, M., RAE, J. W., ZAMELCZYK, K., MARCHITTO, T. M., SZIDAT, S. & SKINNER, L. C. 2021. Deep Ocean storage of heat and CO2 in the Fram Strait, Arctic Ocean during the last glacial period. *Paleoceanography and Paleoclimatology*.

FER, I., BOSSE, A. & DUGSTAD, J. 2020. Norwegian Atlantic Slope Current along the Lofoten Escarpment. *Ocean Science,* 16**,** 685-701.

FOSSILE, E., NARDELLI, M. P., JOUINI, A., LANSARD, B., PUSCEDDU, A., MOCCIA, D., MICHEL, E., PÉRON, O., HOWA, H. & MOJTAHID, M. 2020. Benthic foraminifera as tracers of brine production in the Storfjorden “sea ice factory”. *Biogeosciences,* 17**,** 1933-1953.

FRONVAL, T., JANSEN, E., BLOEMENDAL, J. & JOHNSEN, S. 1995. Oceanic evidence for coherent fluctuations in Fennoscandian and Laurentide ice sheets on millennium timescales. *Nature,* 374**,** 443-446.

GHAFFARI, P., ISACHSEN, P. E., NØST, O. A. & WEBER, J. E. 2018. The influence of topography on the stability of the Norwegian Atlantic Current off northern Norway. *Journal of Physical Oceanography,* 48**,** 2761-2777.

GILBERT, R. 1990. Rafting in glacimarine environments. *Geological Society, London, Special Publications,* 53**,** 105-120.

GODWIN, H. 1962. Half-life of radiocarbon. *Nature,* 195**,** 984.

HAJDAS, I. 2008. Radiocarbon dating and its applications in Quaternary studies. *Eiszeitalter und Gegenwart Quaternary Science Journal,* 57**,** 24.

HANSEN, B. & ØSTERHUS, S. 2000. North atlantic–nordic seas exchanges. *Progress in oceanography,* 45**,** 109-208.

HASS, H. C. 2002. A method to reduce the influence of ice‐rafted debris on a grain size record from northern Fram Strait, Arctic Ocean. *Polar research,* 21**,** 299-306.

HEATHERSHAW, A., HALL, P. & HUTHNANCE, J. 1998. Measurements of the slope current, tidal characteristics and variability west of Vestfjorden, Norway. *Continental shelf research,* 18**,** 1419-1453.

HEBBELN, D., DOKKEN, T., ANDERSEN, E. S., HALD, M. & ELVERHØI, A. 1994. Moisture supply for northern ice-sheet growth during the Last Glacial Maximum. *Nature,* 370**,** 357-360.

HEINRICH, H. 1988. Origin and consequences of cyclic ice rafting in the northeast Atlantic Ocean during the past 130,000 years. *Quaternary research,* 29**,** 142-152.
HENRICH, R., KASSENS, H., VOGELSANG, E. & THIEDE, J. 1989. Sedimentary facies of glacial-interglacial cycles in the Norwegian Sea during the last 350 ka. *Marine Geology,* 86**,** 283-319.
HJELSTUEN, B. O., SEJRUP, H. P., HAFLIDASON, H., NYGÅRD, A., BERSTAD, I. M. & KNORR, G. 2004. Late Quaternary seismic stratigraphy and geological development of the south Vøring margin, Norwegian Sea. *Quaternary Science Reviews,* 23**,** 1847-1865.
HOLTEDAHL, H. 1959. Geology and paleontology of Norwegian Sea bottom cores. *Journal of Sedimentary Research,* 29**,** 16-29.
HOWE, J. N., PIOTROWSKI, A. M., NOBLE, T. L., MULITZA, S., CHIESSI, C. M. & BAYON, G. 2016. North Atlantic deep water production during the last glacial maximum. *Nature communications,* 7**,** 1-8.
JANSEN, E. 1989. The use of stable oxygen and carbon isotope stratigraphy as a dating tool. *Quaternary international,* 1**,** 151-166.
JENNINGS, A. E. & HELGADOTTIR, G. 1994. Foraminiferal assemblages from the fjords and shelf of eastern Greenland. *The Journal of Foraminiferal Research,* 24**,** 123-144.
JESSEN, S. P., RASMUSSEN, T. L., NIELSEN, T. & SOLHEIM, A. 2010. A new Late Weichselian and Holocene marine chronology for the western Svalbard slope 30,000–0 cal years BP. *Quaternary Science Reviews,* 29**,** 1301-1312.
KEIGWIN, L. D. & SWIFT, S. A. 2017. Carbon isotope evidence for a northern source of deep water in the glacial western North Atlantic. *Proceedings of the National Academy of Sciences,* 114**,** 2831-2835.
KENYON, N. H. 1987. Mass-wasting features on the continental slope of northwest Europe. *Marine Geology,* 74**,** 57-77.
KIMOTO, K. 2015. Planktic Foraminifera. *In:* OHTSUKA, S., SUZAKI, T., HORIGUCHI, T., SUZUKI, N. & NOT, F. (eds.) *Marine Protists Diversity and Dynamics.* Springer.
KISSEL, C. 2005. Magnetic signature of rapid climatic variations in glacial North Atlantic, a review. *Comptes Rendus Geoscience,* 337**,** 908-918.
KISSEL, C., LAJ, C., LABEYRIE, L., DOKKEN, T., VOELKER, A. & BLAMART, D. 1999. Rapid climatic variations during marine isotopic stage 3: magnetic analysis of sediments from Nordic Seas and North Atlantic. *Earth and Planetary Science Letters,* 171**,** 489-502.
KNIES, J., KÖSEOĞLU, D., RISE, L., BAETEN, N., BELLEC, V. K., BØE, R., KLUG, M., PANIERI, G., JERNAS, P. E. & BELT, S. T. 2018. Nordic Seas polynyas and their role in preconditioning marine productivity during the Last Glacial Maximum. *Nature communications,* 9**,** 1-10.
KOHFELD, K. E., FAIRBANKS, R. G., SMITH, S. L. & WALSH, I. D. 1996. Neogloboquadrina pachyderma (sinistral coiling) as paleoceanographic tracers in polar oceans: Evidence from Northeast Water Polynya plankton tows, sediment traps, and surface sediments. *Paleoceanography,* 11**,** 679-699.
KRISTJÁNSDÓTTIR, G., LEA, D., JENNINGS, A., PAK, D. & BELANGER, C. 2007. New spatial Mg/Ca ‐ temperature calibrations for three Arctic, benthic foraminifera and reconstruction of north Iceland shelf temperature for the past 4000 years. *Geochemistry, Geophysics, Geosystems,* 8.
KUCERA, M. 2007. Chapter six planktonic foraminifera as tracers of past oceanic environments. *Developments in marine geology,* 1**,** 213-262.

KUIJPERS, A., NIELSEN, T., AKHMETZHANOV, A., DE HAAS, H., KENYON, N. & VAN WEERING, T. 2001. Late Quaternary slope instability on the Faeroe margin: mass flow features and timing of events. *Geo-Marine Letters,* 20**,** 149-159.

LABERG, J., VORREN, T. & KNUTSEN, S.-M. 1999. The Lofoten contourite drift off Norway. *Marine Geology,* 159**,** 1-6.

LABERG, J. S., DAHLGREN, T., VORREN, T. O., HAFLIDASON, H. & BRYN, P. 2001. Seismic analyses of Cenozoic contourite drift development in the Northern Norwegian Sea. *Marine Geophysical Researches,* 22**,** 401-416.

LABERG, J. S. & VORREN, T. O. 2004. Weichselian and Holocene growth of the northern high-latitude Lofoten Contourite Drift on the continental slope of Norway. *Sedimentary Geology,* 164**,** 1-17.

LEKENS, W., SEJRUP, H., HAFLIDASON, H., KNIES, J. & RICHTER, T. 2006. Meltwater and ice rafting in the southern Norwegian Sea between 20 and 40 calendar kyr BP: Implications for Fennoscandian Heinrich events. *Paleoceanography,* 21.

LISIECKI, L. E. & RAYMO, M. E. 2005. A Pliocene‐Pleistocene stack of 57 globally distributed benthic δ18O records. *Paleoceanography,* 20.

LYNCH-STIEGLITZ, J., CURRY, W. B. & SLOWEY, N. 1999. Weaker Gulf Stream in the Florida straits during the last glacial maximum. *Nature,* 402**,** 644-648.

MANGERUD, J., BONDEVIK, S., GULLIKSEN, S., HUFTHAMMER, A. K. & HØISÆTER, T. 2006. Marine 14C reservoir ages for 19th century whales and molluscs from the North Atlantic. *Quaternary Science Reviews,* 25**,** 3228-3245.

MANGERUD, J. & GULLIKSEN, S. 1975. Apparent radiocarbon ages of recent marine shells from Norway, Spitsbergen, and Arctic Canada. *Quaternary Research,* 5**,** 263-273.

MARCOTT, S. A., CLARK, P. U., PADMAN, L., KLINKHAMMER, G. P., SPRINGER, S. R., LIU, Z., OTTO-BLIESNER, B. L., CARLSON, A. E., UNGERER, A. & PADMAN, J. 2011. Ice-shelf collapse from subsurface warming as a trigger for Heinrich events. *Proceedings of the National Academy of Sciences,* 108**,** 13415-13419.

MARGO PROJECT MEMBERS, M. 2009. Constraints on the magnitude and patterns of ocean cooling at the Last Glacial Maximum. *Nature Geoscience,* 2**,** 127.

MCCAVE, I. & HALL, I. R. 2006. Size sorting in marine muds: Processes, pitfalls, and prospects for paleoflow‐speed proxies. *Geochemistry, Geophysics, Geosystems,* 7.

MCCAVE, I., MANIGHETTI, B. & BEVERIDGE, N. 1995. Circulation in the glacial North Atlantic inferred from grain-size measurements. *Nature,* 374**,** 149-152.

MIGEON, S., WEBER, O., FAUGERES, J.-C. & SAINT-PAUL, J. 1998. SCOPIX: a new X-ray imaging system for core analysis. *Geo-Marine Letters,* 18**,** 251-255.

MIX, A. 1987. The oxygen-isotope record of glaciation. *The Geology of North America,* 3**,** 111-135.

MIX, A. C., BARD, E. & SCHNEIDER, R. 2001. Environmental processes of the ice age: land, oceans, glaciers (EPILOG). *Quaternary Science Reviews,* 20**,** 627-657.

NAM, S.-I., STEIN, R., GROBE, H. & HUBBERTEN, H. 1995. Late Quaternary glacial-interglacial changes in sediment composition at the East Greenland continental margin and their paleoceanographic implications. *Marine Geology,* 122**,** 243-262.

Ó COFAIGH, C. & DOWDESWELL, J. A. 2001. Laminated sediments in glacimarine environments: diagnostic criteria for their interpretation. *Quaternary Science Reviews,* 20**,** 1411-1436.

OPPO, D. & LEHMAN, S. 1993. Mid-depth circulation of the subpolar North Atlantic during the last glacial maximum. *Science,* 259**,** 1148-1152.
ORVIK, K. A. & NIILER, P. 2002. Major pathways of Atlantic water in the northern North Atlantic and Nordic Seas toward Arctic. *Geophysical Research Letters,* 29**,** 2-1-2-4.
OTTESEN, D., RISE, L., KNIES, J., OLSEN, L. & HENRIKSEN, S. 2005. The Vestfjorden-Trænadjupet palaeo-ice stream drainage system, mid-Norwegian continental shelf. *Marine Geology,* 218**,** 175-189.
PAWLOWSKI, J., HOLZMANN, M. & TYSZKA, J. 2013. New supraordinal classification of Foraminifera: Molecules meet morphology. *Marine Micropaleontology,* 100**,** 1-10.
PECK, V. L., HALL, I. R., ZAHN, R., ELDERFIELD, H., GROUSSET, F., HEMMING, S. & SCOURSE, J. 2006. High resolution evidence for linkages between NW European ice sheet instability and Atlantic Meridional Overturning Circulation. *Earth and Planetary Science Letters,* 243**,** 476-488.
PISIAS, N., MARTINSON, D., MOORE JR, T., SHACKLETON, N., PRELL, W., HAYS, J. E. & BODEN, G. 1984. High resolution stratigraphic correlation of benthic oxygen isotopic records spanning the last 300,000 years. *Marine Geology,* 56**,** 119-136.
POULAIN, P. M., WARN‐VARNAS, A. & NIILER, P. 1996. Near‐surface circulation of the Nordic seas as measured by Lagrangian drifters. *Journal of Geophysical Research: Oceans,* 101**,** 18237-18258.
PRAETORIUS, S. K., MCMANUS, J. F., OPPO, D. W. & CURRY, W. B. 2008. Episodic reductions in bottom-water currents since the last ice age. *Nature Geoscience,* 1**,** 449-452.
PRELL, W. L., IMBRIE, J., MARTINSON, D. G., MORLEY, J. J., PISIAS, N. G., SHACKLETON, N. J. & STREETER, H. F. 1986. Graphic correlation of oxygen isotope stratigraphy application to the late Quaternary. *Paleoceanography,* 1**,** 137-162.
RAHMSTORF, S. 2002. Ocean circulation and climate during the past 120,000 years. *Nature,* 419**,** 207-214.
RASMUSSEN, T., BÄCKSTRÖM, D., HEINEMEIER, J., KLITGAARD-KRISTENSEN, D., KNUTZ, P., KUIJPERS, A., LASSEN, S., THOMSEN, E., TROELSTRA, S. & VAN WEERING, T. 2002. The Faroe–Shetland Gateway: Late Quaternary water mass exchange between the Nordic seas and the northeastern Atlantic. *Marine Geology,* 188**,** 165-192.
RASMUSSEN, T. L. & THOMSEN, E. 2004. The role of the North Atlantic Drift in the millennial timescale glacial climate fluctuations. *Palaeogeography, Palaeoclimatology, Palaeoecology,* 210**,** 101-116.
RASMUSSEN, T. L., THOMSEN, E., TROELSTRA, S. R., KUIJPERS, A. & PRINS, M. A. 2003. Millennial-scale glacial variability versus Holocene stability: changes in planktic and benthic foraminifera faunas and ocean circulation in the North Atlantic during the last 60 000 years. *Marine Micropaleontology,* 47**,** 143-176.
RASMUSSEN, T. L., THOMSEN, E., VAN WEERING, T. C. & LABEYRIE, L. 1996. Rapid changes in surface and deep water conditions at the Faeroe Margin during the last 58,000 years. *Paleoceanography,* 11**,** 757-771.
REBESCO, M. & CAMERLENGHI, A. 2008. *Contourites,* Elsevier.
REBESCO, M., HERNÁNDEZ-MOLINA, F. J., VAN ROOIJ, D. & WÅHLIN, A. 2014. Contourites and associated sediments controlled by deep-water circulation processes: State-of-the-art and future considerations. *Marine Geology,* 352**,** 111-154.
REIMER, P. J., AUSTIN, W. E., BARD, E., BAYLISS, A., BLACKWELL, P. G., RAMSEY, C. B., BUTZIN, M., CHENG, H., EDWARDS, R. L. & FRIEDRICH, M.

2020. The IntCal20 Northern Hemisphere radiocarbon age calibration curve (0–55 cal kBP). *Radiocarbon,* 62**,** 725-757.
RISE, L., BØE, R., RIIS, F., BELLEC, V. K., LABERG, J. S., EIDVIN, T., ELVENES, S. & THORSNES, T. 2013. The Lofoten-Vesterålen continental margin, North Norway: Canyons and mass-movement activity. *Marine and Petroleum Geology,* 45**,** 134-149.
ROBINSON, S. G., MASLIN, M. A. & MCCAVE, I. N. 1995. Magnetic susceptibility variations in Upper Pleistocene deep‐sea sediments of the NE Atlantic: Implications for ice rafting and paleocirculation at the last glacial maximum. *Paleoceanography,* 10**,** 221-250.
RØRVIK, K.-L., LABERG, J., HALD, M., RAVNA, E. & VORREN, T. 2010. Behavior of the northwestern part of the Fennoscandian Ice Sheet during the Last Glacial Maximum–a response to external forcing. *Quaternary Science Reviews,* 29**,** 2224-2237.
RØRVIK, K. L., RASMUSSEN, T. L., HALD, M. & HUSUM, K. 2013. Intermediate water ventilation in the Nordic seas during MIS 2. *Geophysical Research Letters,* 40**,** 1805-1810.
RUDDIMAN, W. F. 1977. Late Quaternary deposition of ice-rafted sand in the subpolar North Atlantic (lat 40 to 65 N). *Geological Society of America Bulletin,* 88**,** 1813-1827.
RYDNINGEN, T. A., VORREN, T. O., LABERG, J. S. & KOLSTAD, V. 2013. The marine-based NW Fennoscandian ice sheet: glacial and deglacial dynamics as reconstructed from submarine landforms. *Quaternary Science Reviews,* 68**,** 126-141.
SARNTHEIN, M., PFLAUMANN, U. & WEINELT, M. 2003. Past extent of sea ice in the northern North Atlantic inferred from foraminiferal paleotemperature estimates. *Paleoceanography,* 18.
SCHÄFER-NETH, C. & PAUL, A. 2001. Circulation of the Glacial Atlantic: ASynthesis of Global and Regional Modeling. *The Northern North Atlantic.* Springer.
SEIDENKRANTZ, M.-S. 1995. Cassidulina teretis Tappan and Cassidulina neoteretis new species (Foraminifera): stratigraphic markers for deep sea and outer shelf areas. *Journal of Micropalaeontology,* 14**,** 145-157.
SEIDENKRANTZ, M.-S., KUIJPERS, A., AAGAARD-SØRENSEN, S., LINDGREEN, H., OLSEN, J. & PEARCE, C. 2021. Evidence for influx of Atlantic water masses to the Labrador Sea during the Last Glacial Maximum. *Scientific Reports,* 11**,** 1-14.
SEJRUP, H., BIRKS, H., KRISTENSEN, D. K. & MADSEN, H. 2004. Benthonic foraminiferal distributions and quantitative transfer functions for the northwest European continental margin. *Marine Micropaleontology,* 53**,** 197-226.
SESSFORD, E., JENSEN, M. F., TISSERAND, A. A., MUSCHITIELLO, F., DOKKEN, T., NISANCIOGLU, K. H. & JANSEN, E. 2019. Consistent fluctuations in intermediate water temperature off the coast of Greenland and Norway during Dansgaard-Oeschger events. *Quaternary Science Reviews,* 223**,** 105887.
SHACKLETON, N. J. 1977. The oxygen isotope stratigraphic record of the Late Pleistocene. *Philosophical Transactions of the Royal Society of London. B, Biological Sciences,* 280**,** 169-182.
SIMSTICH, J., SARNTHEIN, M. & ERLENKEUSER, H. 2003. Paired δ18O signals of Neogloboquadrina pachyderma (s) and Turborotalita quinqueloba show thermal stratification structure in Nordic Seas. *Marine Micropaleontology,* 48**,** 107-125.

STOW, D. A., KAHLER, G. & REEDER, M. 2002. Fossil contourites: type example from an Oligocene palaeoslope system, Cyprus. *MEMOIRS-GEOLOGICAL SOCIETY OF LONDON,* 22**,** 443-456.
STUIVER, M. & REIMER, P. J. 1993. Extended 14C data base and revised CALIB 3.0 14C age calibration program. *Radiocarbon,* 35**,** 215-230.
SWIFT, J. H. & KOLTERMANN, K. P. 1988. The origin of Norwegian Sea deep water. *Journal of Geophysical Research: Oceans,* 93**,** 3563-3569.
VORREN, T. O. & ELVSBORG, A. 1979. Late Weichselian deglaciation and paleoenvironment of the shelf and coastal areas of Troms, north Norway - a review. *Boreas,* 8**,** 247-253.
VORREN, T. O. & PLASSEN, L. 2002. Deglaciation and palaeoclimate of the Andfjord - Vågsfjord area, North Norway. *Boreas,* 31**,** 97-125.
VORREN, T. O., RYDNINGEN, T. A., BAETEN, N. J. & LABERG, J. S. 2015. Chronology and extent of the Lofoten–Vesterålen sector of the Scandinavian Ice Sheet from 26 to 16 cal. ka BP. *Boreas,* 44**,** 445-458.
VORREN, T. O., VORREN, K. D., AASHEIM, O., DAHLGREN, K. T., FORWICK, M. & HASSEL, K. 2013. Palaeoenvironment in northern N orway between 22.2 and 14.5 cal. ka BP. *Boreas,* 42**,** 876-895.
VORREN, T. O., VORREN, K. D., ALM, T., GULLIKSEN, S. & LØVLIE, R. 1988. The last deglaciation (20,000 to 11,000 BP) on Andoya, Northern Norway. *Boreas,* 17**,** 41-77.
WEFER, G. & BERGER, W. H. 1991. Isotope paleontology: growth and composition of extant calcareous species. *Marine geology,* 100**,** 207-248.
WEINELT, M., SARNTHEIN, M., PFLAUMANN, U., SCHULZ, H., JUNG, S. & ERLENKEUSER, H. 1996. Ice-free Nordic seas during the last glacial maximum? Potential sites of deepwater formation. *Paleoclimates,* 1**,** 283-309.
WEINELT, M., VOGELSANG, E., KUCERA, M., PFLAUMANN, U., SARNTHEIN, M., VOELKER, A., ERLENKEUSER, H. & MALMGREN, B. 2003. Variability of North Atlantic heat transfer during MIS 2. *Paleoceanography,* 18.